CHALMERS
UNIVERSITY OF TECHNOLOGY

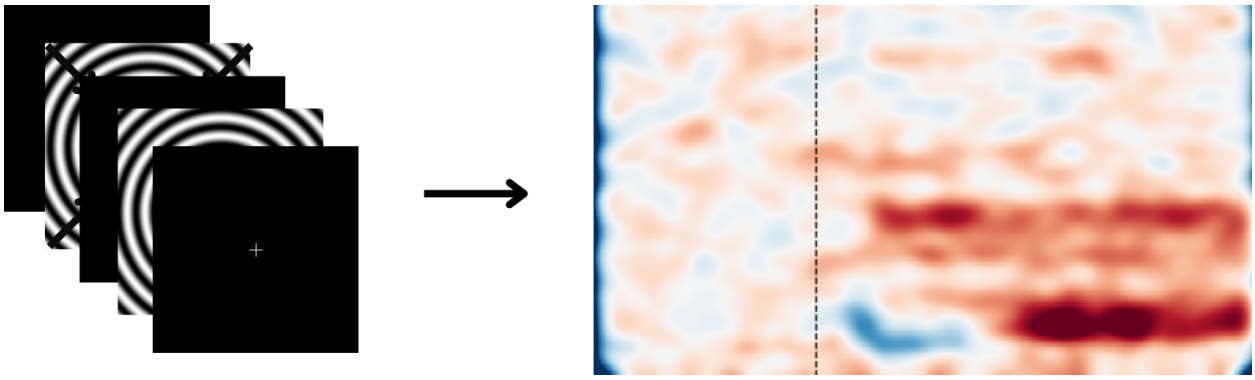

Experimental Protocol for On-Scalp MEG Detection of Gamma Band Neural Oscillations

Master's thesis in Biomedical Engineering

LINA SANDSTRÖM
WILMA SUNNERBERG

DEPARTMENT OF ELECTRICAL ENGINEERING
CHALMERS UNIVERSITY OF TECHNOLOGY
Gothenburg, Sweden 2026
www.chalmers.se

Master's thesis 2026

Experimental Protocol for On-Scalp MEG Detection of Gamma Band Neural Oscillations

LINA SANDSTRÖM
WILMA SUNNERBERG

CHALMERS
UNIVERSITY OF TECHNOLOGY

Department of Electrical Engineering
Division of Signal Processing and Biomedical Engineering
Chalmers University of Technology
Gothenburg, Sweden 2026

Experimental Protocol for On-Scalp MEG Detection of Gamma Band Neural Oscillations
LINA SANDSTRÖM
WILMA SUNNERBERG

Supervisor: Justin Schneiderman, University of Gothenburg
Examiner: Andreas Fhager, Electrical Engineering

Master's Thesis 2026
Department of Electrical Engineering
Division of Signal Processing and Biomedical Engineering
Chalmers University of Technology
SE-412 96 Gothenburg
Telephone +46 31 772 1000

Cover: Visual stimulus of annular gratings generating a neural response in a time-frequency plot.

Typeset in LaTeX
Printed by Chalmers Reproservice
Gothenburg, Sweden 2026

Experimental Protocol for On-Scalp MEG Detection of Gamma Band Neural Oscillations

LINA SANDSTRÖM, WILMA SUNNERBERG
Department of Electrical Engineering
Chalmers University of Technology

Abstract

This thesis developed and validated an experimental visual stimulation protocol intended to induce gamma-band activity in the primary visual cortex. Gamma oscillations are associated with high level cognitive functions, such as sensory perception, problem solving and memory. They are therefore of interest when it comes to neuropsychiatric and neurological disorders, where disruptions in neural processing is often observed. In this context, visually induced gamma oscillations may serve as a useful biomarker to detect altered neural processing in the future.

The aim of this thesis was to implement a visual stimulation paradigm capable of eliciting measurable gamma oscillations. It had to be compatible with the magnetoencephalography (MEG) environment. This included communication and synchronization with an existing acquisition software. In addition, the project involved establishing the visual presentation setup used to display the stimuli in the magnetically shielded room (MSR).

The project encompassed literature studies, design of the stimulus, software development, conducting MEG-recordings and data analysis. Two types of stimulation protocols were implemented. One was based on paradigms identified in the literature, and one that explored a more novel approach to stimulus presentation. The results are promising in terms of integration and synchronization with the existing acquisition software. From the conducted MEG recordings, some indications of gamma activity were observed, although further testing and analysis are required to determine the reliability of these findings. In conclusion, the developed experimental protocol provides a functional basis for future studies investigating visually induced gamma activity.

Keywords: gamma oscillations, visual stimulation, MEG, annular gratings.

Acknowledgements

We want to express our gratitude to our supervisor, Justin Schniederman, whose guidance and advice has been invaluable to us. Thank you for your patience and encouragement when we needed it. We would not have been able to complete this thesis without your continued support and feedback.

We would also like to thank Alessia Garibaldi and Maxim Chukharkin for your guidance, support, and kindness throughout this project. Thank you for brainstorming ideas with us when we got stuck, for allowing us to learn and grow throughout the process, and for involving us in your work on developing the MEG acquisition system. Without you, we would not have come as far with our thesis as we did.

To our examiner, Andreas Fhager, thank you for your valuable feedback on our work and for your support during the final stages of the thesis. Your input helped us improve the quality of the final report, so thank you.

A special thanks also goes to Per-Inge, the carpenter who helped us with the planning and mounting of the projector. Without your help, we would not have been able to complete an important part of the project.

Finally, we would like to thank our friends and families for cheering us on during this semester. Thank you for always listening to us and being there for us.

Lina Sandström, Wilma Sunnerberg, Gothenburg, June 2026

List of Acronyms

Below is the list of acronyms that have been used throughout this thesis listed in alphabetical order:

ASD	Amplitude Spectrum Density
cpd	Cycles per Degree
DAQ	Data Acquisition
ECG	Electrocradiography
EEG	Electroencephalography
EI	Exctiatory-Inhibitory
FFT	Fast Fourier Transform
GABA	Gamma-Aminobutiric Acid
GSS	Gamma Suppression Slope
ICA	Independent Component Analysis
IP	Internet Protocol
IPC	Inter Process Communication
LGN	Lateral Geniculate Nucleus
MEG	Magnetoencephalography
MSR	Magnetically Shielded Room
Perc.	Percentile
PSD	Power Spectral Density
PUB-SUB	Publisher-Subscriber
REQ-REP	Request-Reply
Std	Standard Deviation
SQUID	Superconducting Quantum Interference Device
TCP	Transmission Control Protocol
UDP	User Datagram Protocol
V1	Primary Visual Cortex

Nomenclature

Below is the nomenclature of indices, sets, parameters, and variables that have been used throughout this thesis.

Parameters

α	Visual angle
λ	Spatial wavelength
ϕ	Phase
A	Amplitude of luminance modulation
c	Michelson contrast
d	Viewing distance
f_s	Spatial frequency
L_{max}	Highest luminance
L_{min}	Lowest luminance
W	Width of stimulus

Contents

List of Figures

List of Tables

1

Introduction

The human brain is the central organ of the nervous system responsible for perception, cognition, and the control of behavior [1]. These processes emerge from coordinated electrical signaling across neural networks. Neural activity in the brain can be expressed as rhythmic patterns across distinct frequency ranges. Such rhythmic activity, referred to as neural oscillations, arises from synchronized firing of the neurons in the brain [2].

Neural oscillations are commonly classified into frequency bands, this includes delta, theta, alpha, beta, and gamma [2]. Among these, gamma-band activity is of particular interest because it has been associated with sensory processing, problem solving, and memory formation [3]. At a cellular level, gamma oscillations are believed to depend on the balance between excitatory and inhibitory neuronal activity within the brain [2].

Previous studies have demonstrated that gamma-band oscillations can be reliably induced in the primary visual cortex (V1) using controlled visual stimulation [4–7]. In healthy individuals, the power of the visually induced gamma response has been shown to increase with increasing stimulus intensity. The power then decreases at higher stimulation strengths. This non-linear response is thought to reflect changes in the balance between excitatory and inhibitory neural activity [6]. Disruptions in the EI-balance have been associated with neurological and neuropsychiatric disorders, including autism and schizophrenia [1]. Because of this imbalance, visually induced gamma oscillations may provide a useful biomarker for detecting altered neural processing in these types of conditions [6].

A non-invasive neuroimaging technique that can be used to measure these responses is magnetoencephalography (MEG), which records the weak magnetic fields generated by the synchronized neuronal currents in the brain [8]. Due to its high temporal resolution, MEG is well suited for studying the rapid neural dynamics of gamma-band oscillations [9]. In studies of visually induced gamma activity, MEG can be used to measure changes in gamma power in V1 while participants are presented with controlled visual stimuli [4–7, 10]. This allows the relationship between stimulus intensity, gamma response strength, and excitatory-inhibitory balance to be investigated.

1.1 Research Gap & Motivation

Previous studies have demonstrated that visually induced gamma oscillations can be elicited using discrete stimulation paradigms. Where stimulus properties such as contrast and motion velocity are varied across fixed and separate conditions. However, for such paradigms to be used in MEG studies, they must be implemented in a way that is compatible with the practical and technical requirements of the MEG environment. This includes stimulus presentation, synchronization, and timing accuracy. Therefore, there is a need for a functional and validated visual stimulation protocol that can reliably present visual stimuli during MEG recordings.

The main motivation of this thesis is to develop such a discrete stimulation protocol, providing the research group with a working paradigm for future studies of visually induced neural oscillations. Since gamma-band activity has been associated with visual processing and the EI-balance, this paradigm could support future investigations of altered neural processing in neurological and neuropsychiatric conditions.

In addition to the main discrete protocol, this thesis also explores a continuous stimulation approach. To the best of the author's knowledge, such a protocol has not been implemented in previous studies of visually induced gamma-activity. This approach provides an opportunity to investigate whether gradual stimulus transitions may offer additional information about the non-linear behavior between stimulus strength and gamma power response.

1.2 Aim

The aim of this thesis is to develop a visual stimulation paradigm capable of eliciting measurable gamma-band oscillations in an MEG-compatible environment. The protocol will be implemented as a software framework presenting static and moving annular gratings, with stimulus parameters such as contrast and velocity varied based on previously established findings. Two stimulation approaches will be developed and compared. One discrete protocol, consisting of fixed stimulus conditions, and a continuous protocol where contrast and motion velocity are gradually increased over time.

In addition, a hardware setup for presenting visual stimuli inside a magnetically shielded room will be planned and implemented, ensuring compatibility with MEG measurements while maintaining accurate stimulus timing. The developed system should then be evaluated through pilot testing to assess stimulus visibility, timing accuracy, and overall functionality within the MEG environment.

The intended outcome of the assignment is to have a functional and MEG-compatible visual stimulation protocol, validated through MEG recordings.

1.3 Problem Formulation

- Can a visual stimulation software consisting of static and moving annular gratings be implemented in a way that is compatible with MEG measurements?
- Can two distinct stimulation protocols, one discrete and one continuous, be successfully implemented within the same software framework?
- Will the continuous protocol perform as well as, or better than the discrete during piloting?
- Is the developed hardware setup able to present visual stimuli inside the MEG environment without interference or practical limitations during the measurements?
- Is stimulus timing synchronized with the MEG acquisition system?
- Can the functionality and design of the stimulation protocol be validated through pilot testing, or if MEG measurements are not feasible, through consistency with previously published studies on visual stimulation and gamma-band activity?

1.4 Limitations

The main limitation of this thesis is that the developed stimulation protocol is evaluated through pilot testing rather than a full-scale experimental study. Therefore, the results are primarily intended to demonstrate functionality, feasibility, timing accuracy, and compatibility with the MEG environment. It is not intended to provide statistically robust conclusions about visually induced gamma activity. Since the protocol will only be tested on a limited number of participants, the results cannot be generalized to a broader population without further validation.

Another limitation is that the protocol is constrained by the existing MEG system and hardware setup. The MEG system itself will not be developed or modified as a part of this project, meaning that the performance and testing possibilities depend on the current capabilities and availability of the lab equipment. As a result, the protocol is developed for the specific MEG environment used in this project and may require adjustments if it is to be applied in other laboratories or hardware setups.

Although the protocol is designed to induce gamma-band oscillations, measurable gamma responses may not be clearly observed due to individual variability, technical constraints, or limited recording time. In such cases, alpha-band modulation may still indicate that the visual stimulation engages activity in the visual cortex. If sufficient MEG measurements are not feasible within the project time frame, the protocol cannot be validated through direct measurements of induced gamma activity. The evaluation would then be based on theoretical motivation, technical functionality, and consistency with previous studies on visual stimulation and gamma-band responses.

Furthermore, the thesis is delimited to the development and pilot validation of a MEG-compatible visual stimulation protocol for induced gamma activity. The main

focus is the discrete protocol, while the continuous protocol is included as an exploratory extension. The study does not aim to investigate clinical populations, determine the underlying EI-mechanisms, establish gamma oscillations as a biomarker, or examine gamma activity induced through other sensory modalities. Instead, the purpose is to provide a functional stimulation framework that can be used as a basis for future MEG studies.

2

Theory

This chapter covers the theoretical background necessary for understanding the development and implementation of the stimulation paradigm.

2.1 Neural Oscillations

The human brain consists of 100 billion neurons and an even greater number of connections between them [11]. Pyramidal cells, which are excitatory neurons, are the most common cell type in the cortex. These cells respond to input by exciting other neurons and thereby propagating activity through cortical networks [1, 11]. However, excitation must be carefully regulated in order to support controlled neural processing [11].

This regulation is mediated by inhibitory interneurons, which interact with excitatory pyramidal cells in local cortical circuits [11]. Interneurons limit excessive excitation and help control when and where pyramidal cells are active. The dynamic interaction between excitation and inhibition gives rise to rhythmic patterns of collective neural activity, known as neural oscillations.

Neural oscillations are typically divided into subsets based on the frequency of the oscillations [2]. From lowest to highest frequency range, these are grouped into Delta (0.5-4 Hz), Theta (4-8 Hz), Alpha (8-12 Hz), Beta (13-30 Hz) and Gamma (30-120 Hz) [12]. Preferred oscillatory frequencies differ between structures and states of the brain [2]. These subsets can occur simultaneously in the same or different locations in the brain. Generally, lower frequency oscillations can involve neurons on a more global scale, while high frequency oscillations appear locally [11, 13].

2.1.1 Gamma Oscillations

Gamma oscillations are higher-frequency rhythms that, like other neural oscillations, are thought to depend on interactions between excitatory and inhibitory neurons [14]. Gamma responses are closely associated with GABAergic interneurons, a group of inhibitory neurons that release gamma-aminobutyric acid (GABA), the main inhibitory neurotransmitter in the brain [11, 15]. Since these interneurons are widely distributed throughout the brain, gamma oscillations can arise in many different brain structures [14]. One proposed mechanism is that local inhibitory interneurons rhythmically inhibit excitatory pyramidal cells, thereby aligning their activity in time [15]. This makes excitatory neurons more likely to fire synchronously during

periods when inhibition is reduced. The periodic alternation between inhibition and excitation can therefore give rise to gamma-band rhythmic activity.

Oscillations in the gamma frequency-band are associated with high-level cognitive functions [14], such as sensory perception, problem solving and memory [3]. Gamma signals can therefore be elicited through stimulation of sensory systems, such as the auditory and visual systems [14]. Studies suggest that stimulus features, like contrast, spatial frequency and movement influence the gamma response, while also eliciting notable inter-individual variability [14, 16].

Two common distinctions made when studying stimulus-related activity are evoked and induced oscillations [16, 17]. Evoked oscillations are phase-locked to the stimulus, meaning that they occur with consistent timing across repeated trials. Induced oscillations are also stimulus-related, but their timing or phase varies across trials.

Studies of visual stimulation have shown that gamma activity on the visual cortex is mainly expressed as induced, rather than evoked, oscillatory activity [16]. This non-phase-locked component is the part of the response that varies with stimulus properties. The modulation includes increased amplitude with stimulus contrast and increased frequency with movement of the stimuli. In comparison, increases of the evoked response is mainly affected by changes in stimulus onset or offset and does not show the same difference between stationary and moving stimuli.

Swettenham *et al.* [16] further suggest that increases in gamma frequency may reflect stronger sensory input rather than motion alone. Stronger input may recruit greater inhibitory activity, resulting in higher-frequency gamma oscillations. If gamma frequency is linked to inhibition mediated by GABAergic interneurons, gamma responses may therefore provide an indirect measure of inhibitory processing. This makes visually induced gamma activity relevant as a potential biomarker in conditions where the balance between excitation and inhibition is altered.

It is, however, important to note that the functional consequences of gamma oscillations in sensory perception are still not fully resolved [15]. While gamma activity is closely linked to sensory stimulation and local cortical processing, there is an ongoing debate regarding its exact role in perception. Further understanding of how gamma synchrony is generated and modulated may help clarify this relationship.

2.1.2 Alpha Oscillations

Alpha oscillations are commonly defined as rhythmic activity in the frequency range of 8-12 Hz [11]. However, individual alpha frequency can vary and has been associated with age and sex. Alpha activity is typically described as moderate- to high-amplitude oscillations in posterior cortical regions. Activity appears when relaxed and awake, especially when the eyes are closed [1, 11]. This activity is attenuated by opening the eyes or by increased alertness.

Because alpha activity is prominent over the occipital area, it is often associated with the functional state of the visual cortex [11]. Rather than reflecting visual processing itself, alpha activity has also been interpreted as a rhythm related to disengagement from external sensory input. In visual stimulation experiments, alpha power may

therefore decrease after stimulus onset, reflecting a shift from a relaxed or disengaged state toward active sensory processing [1, 11].

Although alpha and gamma oscillations occupy different frequency ranges, they are not mutually exclusive. Slower alpha activity can modulate faster gamma-band activity, and the connection between these rhythms has been suggested to have perceptual relevance [11]. However, during sensory stimulation, alpha activity is often reduced, while gamma-band activity may be induced or enhanced. This makes it relevant to consider both frequency bands when analyzing visually induced neural responses.

2.1.3 Techniques for Recording Neural Oscillations

In order to study the different rhythms of the brain, there are two common non-invasive recording techniques. Electroencephalography (EEG) and MEG record electrical fields and magnetic fields in the brain respectively [13]. These signals stem from the same main source. When pyramidal cells fire, both electrical and magnetic fields are generated. Thus, when a multitude of neurons activate synchronously, this gives rise to local field potentials and local magnetic fields, which can be detected and recorded outside the skull.

The signal generated by the neurons have to pass through several layers of tissue to reach the sensors [13]. Therefore, the signal is attenuated and distorted between the source and the sensors. This is more pronounced in EEG recordings, since these conductive layers influence the electric field far more than the magnetic field. Because of this, MEG is less affected by the conductive properties of the tissue between the neural source and the sensors. This allows neural activity to be measured with a very high temporal and spatial resolution with a MEG system [9].

Recording MEG signals is challenging on account of the extremely small magnetic fields generated by synchronized brain activity [18, 19]. Therefore, sensitive sensors are essential for detecting these weak signals. Superconducting Quantum Interference Devices (SQUIDs) are utilized in most cases. In order for the SQUIDs to become superconducting, they have to be cryogenically cooled. This is most commonly achieved by placing the sensors inside tanks filled with either liquid helium or liquid nitrogen [19]. With the high sensitivity of SQUIDs, they are also highly sensitive to magnetic noise [18, 19]. Since the magnetic fields generated by the brain are extremely small, most interfering magnetic fields are stronger. In order to mitigate magnetic noise, MEG recordings have to be conducted inside a magnetically shielded room (MSR).

Because MEG sensors are not fixed to the scalp, even small head movements affect the recordings [18]. This is not the only source of artifacts. Blinking, eye movements, heartbeats and small muscle contractions can also introduce artifacts in the recording, and can be mitigated through signal processing techniques [19]. In addition to this ferromagnetic artifacts are also common, since any movement of a magnetizable object is picked up by the sensors [18]. This can be more obvious objects, like pacemakers or orthodontic braces, but it can also be less obvious ones, like metallic particles in makeup or hair products. Ferromagnetic artifacts can be

difficult to remove after recording, making it important to minimize their presence before data acquisition begins.

2.2 Pre-Processing & Spectral Analysis

The purpose of the analysis pipeline is to extract stimulus-related changes in oscillatory activity from the recorded MEG signal [19]. This involves first reducing noise and artifacts, then segmenting the data relative to stimulus events, and finally estimating spectral and time-frequency power [20].

Since MEG recordings are sensitive to both environmental noise and physiological artifacts, the measured signal cannot be interpreted directly as neural activity. These artifacts must be reduced or excluded before stimulus-related responses can be analyzed [19]. Preprocessing is therefore an essential step between data acquisition and the estimation of alpha- and gamma-band activity.

A common first step in preprocessing is filtering [21]. It is used to attenuate unwanted frequency components while preserving the frequencies relevant to the analysis. Line noise from electrical equipment can appear as strong activity at specific frequencies (50 Hz in Sweden) and can be reduced with a notch filter [19]. Band-pass filtering is then used to retain the frequency range of interest, while removing the lower and higher-frequencies that are not of interest.

In addition to filtering, noisy SQUIDs and artifact-contaminated time periods can be marked through annotation [21]. Channels with excessive noise may be excluded from further analysis, while annotated time segments can be omitted in later steps. Physiological artifacts, such as those caused by eye movements, blinking, muscle contractions, and the heartbeat, can also be reduced using methods such as independent component analysis (ICA). ICA separates the recorded signal into components with different spatial and temporal patterns, allowing components related to artifacts to be identified and removed before reconstructing the cleaned signal [19]. This cleaning method is most efficient when additional recordings like electrocardiography (ECG) and EEG are also included.

After preprocessing, the entire recording is typically divided into epochs [22]. These are short time windows extracted around specific events, such as the onset of a stimulus. This makes it possible to compare neural activity before and after stimulation and to average responses across repeated presentations of the same stimulus condition.

When studying stimulus-related activity, an important distinction is made between evoked and induced responses [17]. As previously mentioned, evoked activity is phase-locked to the stimulus. Because of this, it remains visible when epochs are averaged in the time domain. Induced activity is not phase-locked across trials. Since its timing or phase can vary between epochs, it will cancel out during direct averaging of the time-domain signal.

To study the induced activity, oscillatory power must therefore be estimated separately for each epoch before averaging across them [23]. This is commonly done using time-frequency analysis, which shows how power changes over time within different

frequency bands. The resulting power contains both phase-locked and non-phase-locked components. The induced component can then be estimated by removing the phase-locked evoked contribution from the total time-frequency power.

Spectral analysis can be used to inspect the frequency content of the signal [19]. Methods such as fast Fourier transform (FFT) or power spectral density (PSD) estimation show how signal power is distributed across frequencies [24]. These methods are useful for identifying dominant oscillatory frequencies, such as alpha or gamma activity, but they do not preserve detailed information about when changes in power occur relative to the stimulus.

Time-frequency analysis addresses this limitation by estimating power as a function of both time and frequency. One common approach is Morlet wavelet decomposition, where the signal is compared with short oscillatory wavelets at different frequencies [19, 24]. This makes it possible to examine how alpha- and gamma-band power change over the course of each epoch. The number of cycles in the wavelet determines the trade-off between temporal and frequency resolution. Fewer cycles provide better temporal resolution but poorer frequency resolution, whereas more cycles does the opposite.

Finally, time-frequency power is often expressed relative to a pre-stimulus baseline [19, 24]. Baseline correction reduces the influence of differences in absolute signal power between channels, participants, or conditions. By comparing post-stimulus power to activity before stimulus onset, stimulus-related increases or decreases in oscillatory power can be more clearly interpreted.

2.3 Visual Processing

The early visual system transforms incoming light into structured neural representations through a hierarchical pathway consisting of the retina, the lateral geniculate nucleus (LGN) and the primary visual cortex (V1) [1], as illustrated in Figure 2.1. This pathway preserves the spatial organization of the visual field, enabling precise and localized responses to visual input.

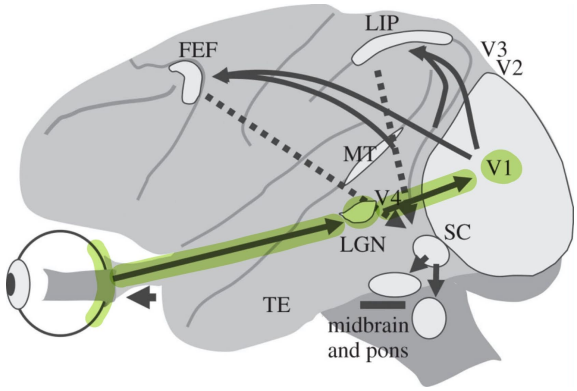

Figure 2.1: Hierarchical visual pathway from the retina to the lateral geniculate nucleus (LGN) and primary visual cortex (V1). Green highlights were added to distinguish the visual pathway. Adapted from [25], CC BY 4.0.

In the retina, neural circuits enhance contrast and spatial differences in the visual scene before transmitting signals to the LGN [1]. The LGN relays this information to V1 while maintaining retinotopic organization, ensuring that neighboring points in visual space activate neighboring cortical neurons.

The primary visual cortex represents the first cortical stage of visual processing [1]. Neurons in V1 respond selectively to stimulus features such as orientation, spatial frequency, contrast, and motion. This feature-specific organization is supported by dense local networks of excitatory pyramidal cells and inhibitory interneurons. The interaction between these cell populations enables regulated and synchronized activity.

Following stimulus presentation, neural responses are not observed instantaneously, but occur after a short processing delay [3]. In visual tasks, responses are commonly expected within the first few hundred milliseconds after stimulus onset, with a typical reaction time of approximately 200 ms. This temporal delay is important to consider when relating stimulus events to measured MEG responses.

Since V1 responses are strongly modulated by well-structured stimulus parameters, visual input can reliably and systematically drive local cortical circuits [1]. This makes the early visual cortex particularly suitable for studying stimulus-induced gamma-band oscillations under controlled experimental conditions.

2.4 Stimulus Properties & Spatial Processing

Given the structured organization and stimulus dependence of V1, visual stimulation provides a controlled method for modulating gamma-band activity [1]. Because neural responses in early visual cortex are tightly linked to external input, stimulus-induced activity can be systematically manipulated by varying defined properties of the visual signal.

In experimental settings, visual stimuli are commonly presented as sinusoidal gratings [26]. A one-dimensional sinusoidal luminance pattern can be described as this following sine wave,

$$f(x) = A \sin\left(\frac{2\pi x}{\lambda} + \phi\right), \tag{2.1}$$

where A represents the amplitude of the luminance modulation, λ denotes the spatial wavelength, and ϕ represents the phase of the pattern. Although the grating is defined in physical units on a display, the visual system responds to the retinal image it produces. The relevant measure for spatial vision is therefore the visual angle that the stimulus spans on the retina [27]. For a stimulus of width W presented at a viewing distance d, the visual angle α is given by the following equation

$$\alpha = 2 \arctan\left(\frac{W}{2d}\right), \tag{2.2}$$

where α is expressed in radians. This relationship allows conversion between physical

stimulus dimensions and their corresponding retinal projection.

Because neurons in V1 are tuned to specific frequencies, defined in terms of visual angle, spatial frequency is typically expressed in cycles per degree (cpd) rather than cycles per unit length of the display [27]. The spatial frequency of the stimulus, expressed in cpd, is given by the inverse of the wavelength when measured in degrees of visual angle, see Eq. 2.3.

$$f_s = \frac{1}{\lambda} \tag{2.3}$$

The amplitude parameter, A in Eq. 2.1, is directly related to stimulus contrast. Contrast quantifies the relative difference between the maximum and minimum luminance values of an image [27]. It is commonly defined using the Michelson contrast,

$$c = \frac{L_{max} - L_{min}}{L_{max} + L_{min}}, \tag{2.4}$$

where L_{max} and L_{min} represent the highest and lowest luminance values of the stimulus, respectively. The contrast parameter ranges from 0 to 1, where 0 indicates no luminance difference and values approaching 1 represent maximal contrast.

In addition to spatial properties, motion can be introduced by varying the phase of the sinusoidal grating over time [27]. A continuous shift in phase produces a drifting grating, and the rate of phase change determines the temporal frequency or motion velocity of the stimulus. By manipulating contrast and motion velocity, the strength and temporal dynamics of excitatory drive to V1 can be systematically controlled [1].

2.5 Prior Work of Visual Gamma Stimulation

Previous research has demonstrated that structured visual stimuli can induce gamma-band oscillations in the primary visual cortex. These responses have been shown to depend on stimulus parameters such as contrast, spatial frequency and motion velocity. This section presents selected work that has shown promising results in this field of visually induced gamma activity.

2.5.1 Effects of Stimulus Design on Visual Gamma Responses

In 2013, S. Muthukumaraswamy and K. Singh [26] investigated how specific stimulus design features influence visually induced gamma activity measured with MEG and EEG. They compared eight different grating configurations that varied in stimulus type (annular vs. square-wave), visual field coverage (one quadrant vs. four quadrants), and motion (stationary vs. drifting). All stimuli were presented at high contrast and with a spatial frequency of 1 cycle/degree.

Their results showed that annular gratings elicited stronger gamma responses than square-wave gratings. Stimulating all four visual quadrants elicited greater gamma

power than stimulating a single quadrant. Drifting gratings generated both stronger gamma amplitudes and higher peak frequencies compared to stationary stimuli. Moreover, MEG proved substantially more sensitive to gamma-band activity than EEG.

Importantly, conditions that elicited stronger gamma power also yielded more reliable peak frequency estimates. The upward shift in peak frequency observed for moving stimuli suggests that gamma frequency may reflect changes in the balance between excitation and inhibition within local cortical circuits.

Overall, this study highlights that stimulus configuration critically shapes both the amplitude and frequency of visually induced gamma oscillations. It emphasizes the importance of careful stimulus design in experimental paradigms.

2.5.2 Gamma Suppression & Excitation-Inhibition Balance

Orekhova and colleagues [4–7] have systematically investigated how visually induced gamma oscillations depend on the strength of sensory input. Across a series of MEG studies, they employed a consistent experimental paradigm where the participants viewed high-contrast annular gratings on a black background. The gratings drifted inward toward the center at three velocities, referred to as low, medium, and high velocity. The main visual stimulus parameters are summarized in Table 2.1.

Table 2.1: Visual stimulus conditions used in the experimental paradigm described by Orekhova et al. [4–7].

Condition	Velocity	Temporal frequency	Spatial frequency
Low velocity	1.2°/s	2 Hz	1.66 cycles/°
Medium velocity	3.6°/s	6 Hz	1.66 cycles/°
High velocity	6.0°/s	10 Hz	1.66 cycles/°

Stimuli were high-contrast annular gratings with an outer diameter of 18° visual angle.

Each trial began with a white fixation cross on a black background, presented for 1200 ms [4–7]. The drifting grating was then displayed for a randomized duration between 1200 and 3000 ms. Participants were instructed to press a button as soon as the motion stopped. If no response occurred within 1 second, a discouraging message ("too late!") appeared for 2000 ms before the next trial. Responses that were either too early (less than 150 ms after motion offset) or too late were classified as error trials and excluded from the analysis. Each stimulus condition was presented in three experimental blocks in a randomized order, with each type repeated 30 times per block, resulting in 90 repetitions per condition across the experiment. Short animated cartoons were presented for 3-6 seconds after every 2-5 trials to reduce fatigue and maintain vigilance.

This paradigm provides a controlled approach to examine how increasing excitatory drive influences gamma frequency and power. It served as the basis of the experimental paradigm, which was adjusted to examine new specific hypotheses in

subsequent studies.

Using this approach, their initial study demonstrated that gamma activity can be systematically modulated by motion velocity [4]. Gamma frequency increased monotonically with velocity, whereas gamma power followed a bell-shaped profile, increasing with low to moderate velocities but decreasing at higher velocities. This suppression effect was robust across participants and was replicated in both adults and children. The authors interpreted this patten as reflecting inhibitory gain control, where excessive excitatory input leads to over-recruitment of inhibitory neurons and a breakdown of neural synchrony. It is notable that the relative magnitude of suppression remained stable across development, suggesting some preservation of the functional EI-balance.

Building on these findings, their next study examined whether gamma suppression related to individual differences in sensory sensitivity between two groups, where one group consisted of neurotypical adults and the other adults with autism spectrum disorder [5]. Sensory sensitivity was assessed using the Adolescent/Adult Sensory Profile prior to MEG recordings. To quantify the velocity-dependent gamma suppression, the authors introduced the Gamma Suppression Slope (GSS) index, which measures the change in gamma power across stimulus velocities. More negative GSS values indicate stronger suppression and are interpreted as reflecting more inhibitory gain control in the primary visual cortex.

The results showed that individuals with higher sensory sensitivity exhibited weaker gamma suppression (less negative GSS) at high motion velocities [5]. Importantly, this relationship was continuous across participants and not specific to diagnostic group, indicating that gamma suppression reflects a trait-like property of cortical function. These findings link inhibitory gain control in the visual cortex to perceptual experiences in everyday life.

To further clarify the underlying mechanism, a later study investigated the combined effects of contrast and motion velocity on gamma activity [6]. While increasing contrast led to a monotonic increase in gamma power, motion velocity again elicited a non-linear modulation, with suppression emerging at high velocities. These effects were additive, such that suppression at high velocities was stronger under high-contrast conditions. This demonstrates that both modulations increase excitatory drive. It also supports the interpretation that gamma suppression reflects a breakdown of synchrony under excessive excitation rather than reduced sensory input. Consistent with this, gamma frequency continued to increase with velocity even when gamma power decreased, indicating sustained excitatory input despite reduced synchronization. Moreover, individual differences in GSS were preserved across conditions, suggesting a common underlying mechanism related to the EI-balance.

To further validate the functional significance of gamma suppression, a later study examined its relationship to spatial suppression in motion perception [7]. Spatial suppression refers to the reduced ability to discriminate the direction of motion for large, high-contrast stimuli compared to smaller ones, a phenomenon thought to reflect inhibitory interactions from surrounding visual inputs in primary visual cor-

tex. Participants completed both a psychological motion discrimination task and the MEG paradigm described above. In the behavioral task, they judged the direction of drifting gratings of different sizes, allowing estimation of spatial suppression strength. In parallel, gamma responses were measured across motion velocities, and the GSS was computed as an index of velocity-dependent attenuation of gamma power.

The results revealed a strong and selective relationship between neural and behavioral measures [7]. Individuals with more negative GSS, indicating stronger gamma suppression, exhibited stronger inhibitory surround mechanisms. This relationship was replicated across independent samples of adults and children and was stable across repeated testing sessions. No association was found for small stimuli, supporting the specificity of the effect.

Together, these findings provide evidence that velocity-dependent gamma suppression reflects the efficiency of inhibitory processing in the visual cortex. By linking stimulus-driven neural dynamics to both individual differences in sensory sensitivity and perceptual performance, this body of work establishes gamma suppression as a potentially robust, non-invasive marker of the EI-balance in the human brain.

2.6 Software

Software plays a central role in experimental neuroscience because it supports both experimental control and offline data analysis [28]. In visual stimulation experiments, software is used to define and present stimuli with controlled timing and visual properties, while analysis software is used to preprocess recorded signals and estimate neural responses. The Python library PsychoPy provides tools for creating neural experiments, including visual stimulus presentation [28]. For the analysis, MNE-Python provides functions to create a complete analysis pipeline for MEG data [20].

Due to the usability of PyschoPy and MNE, Python is a suitable programming language. It provides a flexible programming environment with many libraries for numerical computation, data handling, visualization, and signal processing.

PsychoPy is an open-source software package for designing and running experiments in psychology and neuroscience [28]. It allows visual stimuli to be defined using parameters such as size, position, contrast, spatial frequency, phase, and temporal dynamics. This makes it suitable for implementing controlled visual stimulation paradigms.

MNE-Python is also an open-source software package used for analyzing MEG and EEG data [20]. It provides tools for loading the recordings, filtering, epoching, artifact handling, spectral analysis, as well as time-frequency analysis. These functions are essential for studying neural oscillations because they allow signal power to be estimated within specific frequency bands and time windows.

2.7 Data Communication

For experiments involving separate stimulation and recording systems, software communication and synchronization are very important. There are multiple ways to send messages from one system to another. Depending on application and requirements, some are more suitable than others. A common mechanism is Inter Process Communication (IPC), that allows processes on the same device to send messages between each other [29]. IPC enables fast and efficient communication between local processes [29, 30]. However, in cases where communication between computers is necessary, communication protocols based on the Internet Protocol (IP) are commonly used [31].

The Internet Protocol describes how messages can be sent to their destination [32]. It does so by splitting the message into packets and sending the packets without handling the order, content or origin of them. To deal with these problems, higher level protocols can be used on top of IP. Two common alternatives are User Datagram Protocol (UDP) and Transmission Control Protocol (TCP). UDP solves the problem with corrupt packets, meaning that the content of the packet is intact [33]. However, they can still arrive out of order. This makes it a simple but fast protocol compared to TCP. TCP is the protocol most commonly used on top of IP [32] and solves many of its issues [34]. It provides reliable and ordered delivery to the recipient. These properties make TCP suitable for a variety of applications where speed cannot compensate for reduced reliability.

2.7.1 ZeroMQ

ZeroMQ is a messaging library that can be used in various programming languages, including Python [35]. It is designed to provide low-latency messaging that is communicated directly between endpoints. The library supports multiple transport types, such as TCP, interprocess communication, and multicast, among others. ZeroMQ uses sockets to send messages across the various transports. These sockets work together in so called messaging patterns, where different types of sockets are paired together.

Two common socket pairs are Request-Reply (REQ-REP) and Publish-Subscribe (PUB-SUB) [35]. Both of these have one socket that sends messages, the Request and Publish sockets, and a socket that receives the message (Reply and Subscribe sockets). However, they differ in how they handle messages. The PUB-SUB pattern have no back-chatter, the message is sent from the publisher to the subscriber, but no confirmation that the message was received is sent back. This simplifies the message flow but introduces the risk of dropping messages if the subscriber cannot keep up with the publisher. In contrast to the PUB-SUB pattern, REQ-REP enforces a strict send-receive alteration. A REQ socket cannot transmit a subsequent request until a reply has been received from the REP socket. This introduces blocking behavior, since the communication depends on both sides completing their part of the exchange before the next message can be sent. While this can be useful when confirmation or synchronization is required, it may be less suitable in situations

where one process needs to continue running without interruption.

3

Methods & Materials

This chapter describes the methods and materials used to design, implement, and evaluate the experimental paradigm. The aim was to develop a visual stimulation setup suitable for MEG measurements of stimulus-induced gamma activity. The setup consisted of both software and hardware components, including the visual stimulation software, synchronization and trigger registration, a display and mirror system, participant positioning, and pilot testing of the complete system.

The experimental paradigm was implemented as a visual stimulation software with two main protocols, a discrete and a continuous. In addition, a gamma localization protocol was initiated with the purpose of getting better positioning of the sensors during MEG-recordings.

Since the setup was intended for use in a particular MEG environment, the experimental design also had to account for practical constraints related to the size of the MSR, stimulus presentation, timing accuracy, and synchronization with the MEG acquisition system. The software and hardware components were therefore interconnected with each other. The stimulation software controlled the visual stimuli, trigger events were used to synchronize stimulus timing with the recorded MEG data, and the display and mirror system determined how the stimuli were presented to the participant inside the MSR.

The following sections describe each component of the setup in the order in which it contributed to the experimental workflow. Starting from stimulus design and software implementation to MEG synchronization, hardware configuration, pilot testing, and data analysis.

3.1 Visual Stimulus Design

The visual stimuli used in this project consisted of annular gratings, defined according to Eq. 2.1, with a spatial frequency of 1.66 cpd. These stimuli were designed to induce gamma-band oscillations in the primary visual cortex. Annular gratings were selected based on previous studies demonstrating that visual gratings can elicit measurable gamma responses [10]. The stimulus paradigm developed in this project was based on similar visual gamma paradigms, but was adapted to fit the existing seven channel MEG system [4–7].

Across the implemented protocols, seven stimulus conditions were used. Three of these conditions were static and differed only in contrast. The contrast levels were

defined using the Michelson contrast and were referred to as low_c, med_c, and high_c, where c denotes contrast. Three additional conditions consisted of moving gratings with fixed contrast but different motion velocities. These conditions were referred to as low_m, med_m, and high_m, where m denotes motion. The final condition consisted of a gradual increase in contrast followed by a gradual increase in motion velocity, all happening within a single stimulus epoch. This condition is referred to as cont. The parameter values for all stimulus conditions are shown in Table 3.1. An illustration of the annular gratings can be found in Figure 3.1.

Table 3.1: Overview of contrast and motion stimulus parameters used in the discrete and continuous protocols.

Condition	Contrast	Velocity [$^\circ/s$]	Temporal Frequency [Hz]
low_c	0.1	0	0
med_c	0.5	0	0
high_c	1	0	0
low_m	1	1.2	2
med_m	1	3.6	6
high_m	1	6.0	10
cont	[0, 1]	[0, 6.0]	[0, 10]

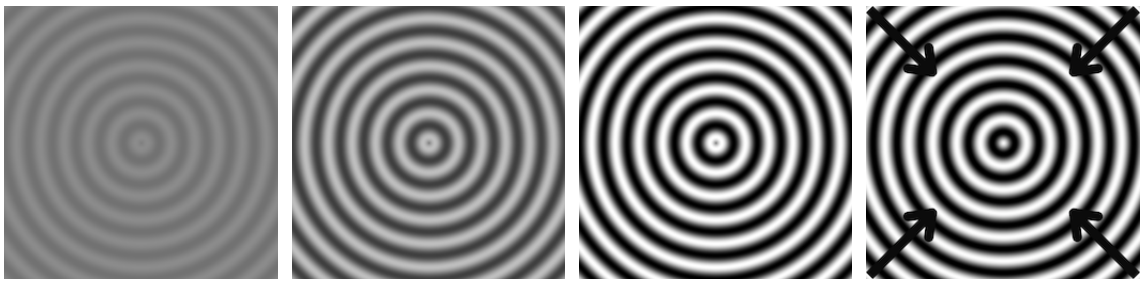

(a) (b) (c) (d)

Figure 3.1: Annular gratings corresponding to the different conditions used for the visual stimulation. The first three images (a-c) depict the static gratings, low_c, med_c and high_c from left to right. (d) Moving annular grating, where the arrows indicate the direction of motion.

The stimuli were presented centrally on a black background and alternated with a fixation cross. For all protocols, the duration of each stimulus presentation was randomized within a predefined interval. The interval differed between the discrete and continuous protocols, as the protocols had different timing requirements. A fixation duration of 1.2 s was used for both protocols. To reduce fatigue and provide short periods of visual rest, an animated image was displayed after every n:th stimulus presentation. This image was shown for a fixed duration of 5 s in both protocols. The main timing parameters, including stimulus duration, fixation duration and break frequency could be adjusted through the user interface.

To encourage the participant to maintain attention on the screen, a button-press task was included during the fixation periods. The participant was instructed to press a button whenever the fixation cross was displayed. For the response to be accepted, the button press had to occur within a predefined time interval of 0.15 to 1.0 s. These limits were determined with prior studies in mind [4–7]. If the participant responded too early, too late or failed to respond, feedback was displayed on the screen. A response that occurred before the accepted interval resulted in the message "Too Fast!", whereas a missing or delayed response resulted in the message "Too Slow!". Trials with missed or invalid responses were added back to the end of the protocol to ensure that the final number of accepted trials was balanced across stimulus conditions.

3.1.1 Discrete Protocol

The discrete paradigm consisted of the first six stimulus conditions described previously in table 3.1 (low_c, med_c, high_c, low_m, med_m, high_m). These conditions represented fixed combinations of contrast and motion velocity. In each trial, one stimulus condition was presented and the stimulus parameters remained constant throughout the stimulation period. Each trial consisted of a fixation cross followed by one stimulus presentation. The duration of the stimulus was randomly selected from a predefined interval between 1 and 3 seconds, while the fixation duration was set separately to 1.2 seconds, an illustrative example of this protocol can be seen in Figure 3.2.

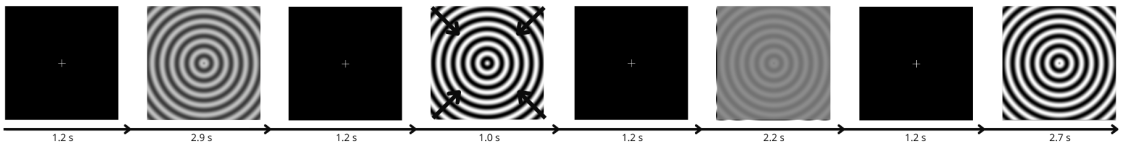

Figure 3.2: Short illustration of how the discrete protocol can look over a timeline. A fixation cross is displayed between every stimulus condition. The stimulus with arrows indicates a moving grating, while stimuli without arrows are static.

The protocol was implemented with an adjustable trial structure. The number of repetitions per condition, the number of blocks, timing parameters, as well as which stimulus conditions to include could be modified through the user interface, which is explained further in Section 3.2. This was done to allow the protocol duration and overall structure to be adapted during pilot testing, since the number of trials required to obtain a measurable gamma-band response with the existing MEG system was not known before.

Within each block, the order of stimulus presentation was randomized to reduce expectation effects. Each stimulus condition was therefore distributed throughout the block rather than being presented in a fixed sequence. To reduce fatigue, an animated image was displayed after every n:th stimulus presentation for a predefined duration of 5 s. However, the frequency and duration of these breaks could also be adjusted as needed through the interface.

The discrete protocol was used both as a structured stimulation paradigm and as a pilot tool for evaluating whether visually induced gamma-band activity could be detected with the available MEG setup.

3.1.2 Continuous Protocol

The continuous protocol followed the same general presentation structure as the discrete protocol, with alternating fixation and stimulation periods. Participants were instructed to respond to the transition between the stimulus and fixation cross using the same button-press task as in the discrete protocol. An animated image was also presented after every n:th stimulus presentation for a fixed duration of 5 s.

In contrast to the discrete protocol, the continuous protocol consisted of one stimulus condition in which the contrast and motion velocity changed gradually within each stimulation period, see Figure 3.3 for an illustration of this stimulus condition. Each stimulus presentation started with a static annular grating with contrast $c = 0$. The stimulus then remained static for a predefined duration, where the contrast increased linearly until full contrast was reached. After this, the grating started drifting inward, and the motion velocity increased linearly until the maximum temporal frequency of 10 Hz was reached.

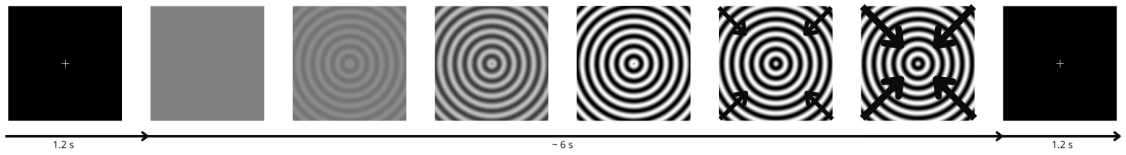

Figure 3.3: Illustration of a continuous stimulus epoch. A fixation cross is displayed between each stimulus epoch. The stimulus starts as a low contrast static grating, the contrast is then increased until full contrast is reached. At this point, the grating starts drifting with increased velocity, denoted by the increased size of the arrows.

The timing of these transitions was based on the shortest possible stimulus duration in the continuous protocol. The contrast increase occupied the first third of this minimum duration, while the velocity increase occupied the remaining two thirds. This division was chosen so a greater part of the epoch involved motion, since previous studies have shown that high-contrast moving gratings yields stronger gamma responses. Once the maximum temporal frequency of 10 Hz had been reached, the motion velocity remained constant for the rest of the stimulation period. The reason for this design choice was to simplify the alignment of contrast and velocity changes when creating epochs in the signal analysis. This is described in further detail in section 3.5 about the analysis.

Considering that several stimulus states were included within the same stimulation period, the continuous protocol required a longer stimulus presentation than the discrete protocol. The stimulus duration was therefore randomized within a longer time interval.

The continuous protocol was also implemented with adjustable timing and sequence

parameters. The stimulus duration interval, fixation duration, number of epochs, number of blocks, break frequency and duration of the initial static period could be modified through the user interface. This flexibility allowed the protocol to be adapted during pilot testing, both in terms of total recording time and participant tolerance.

3.1.3 Gamma Localization Protocol

In addition to the discrete and continuous protocols, a preliminary localization protocol was also established. The idea behind this protocol is to use it as a first step in a recording to verify that the placement of the sensors are correct. This protocol consisted of one single discrete stimulus condition, low_m, as this state has consistently yielded the highest gamma power response [4–7].

Since this protocol is supposed to be used as a quick verification of sensor placement, it is simplified significantly in comparison to the full-scaled discrete and continuous protocols. It therefore consists of one block, with a fewer number of repetitions for the single stimulus condition. From here, a block refers to a series of stimuli conditions, while a single stimulus is referred to as an epoch or a trial.

3.2 Software Implementation

The visual stimulation software was developed to control stimulus generation, stimulus presentation, participant responses, trigger communication and experimental logging. The software was implemented in Python and was designed to allow flexible adjustment of protocol parameters while maintaining frame-based stimulus timing.

3.2.1 Interface & Protocol Setup

The stimulation software was controlled through a graphical user interface implemented using the package PyQt6 [36]. The interface was designed to allow the user to select and configure the stimulation protocol without having to modify the source code. When the program was started, the user was first presented with a short description of the available protocols and could choose between the continuous, discrete and localization protocols. After a protocol had been selected, the interface displayed the parameter fields relevant to that protocol.

The adjustable parameters included the monitor used for stimulus presentation, number of blocks, stimulus duration mode, fixation duration, number of stimulation epochs, temporal frequency, spatial frequency and pause settings. The stimulus duration could either be fixed or randomized within a selected interval. For the continuous protocol, the user specified the highest temporal frequency reached during the stimulus presentation. For the discrete protocol, separate low, medium and high temporal frequencies were specified. An optional stimulus-type selection was also included for the discrete protocol, allowing individual stimulus conditions to be included or excluded before starting the protocol.

After parameter selection, the interface collected the chosen values and passed them to the corresponding stimulation function and instructed them to begin. After completion of the discrete and continuous protocols, a log window was displayed. This log summarized the selected parameters, block durations, epoch durations, response information, frame rate, and total protocol duration, and could also be saved as a text file for later documentation.

3.2.2 Visual Stimulus

Before each protocol started, the visual elements required for that protocol were generated and stored. This included the fixation cross, annular gratings, feedback messages, break images and visual trigger markers. Stimulus images were created as PsychoPy ImageStim objects, allowing them to be drawn directly during the frame-by-frame presentation loop. Pre-generating the visual stimuli reduced the amount of computation required during stimulus presentation and helped with maintaining stable timing.

Annular gratings were generated numerically using a sinusoidal function of the radial distance from the image center. First, a two-dimensional coordinate grid was created and converted into a radial distance matrix. This matrix was then used to calculate the grating intensity as a function of wavelength, phase, and contrast. Static gratings were created by keeping the phase constant, whereas moving gratings were created by generating a sequence of images with gradually increasing phase.

Stimulus presentation and timing was implemented using a frame-based presentation loop, see Listing 3.1 for pseudo code. For each trial, the number of frames corresponding to the selected stimulus duration was calculated from the display refresh rate. This stimulus was then drawn and updated once per frame before the display buffer was flipped. This approach allowed stimulus duration, image transitions and phase updates to be synchronized with the refresh cycle of the display.

Listing 3.1: Frame-based drifting grating update.

```
For each frame in stimulus duration
    Calculate current phase
    Generate grating image using contrast and phase
    Draw stimulus
    Flip Display
    Update phase
```

For the discrete protocol, a stimulus schedule was generated at the beginning of each block, see Listing 3.2. The schedule contained the selected stimulus conditions repeated according to the chosen number of repetitions per condition. The order was randomized within each block so that conditions were distributed across the recording. If a participant response was classified as invalid or missing, the corresponding trial was added back to the schedule to preserve the intended number of accepted trials per condition.

Listing 3.2: Discrete Protocol Pipeline.

```
Create empty schedule
For each slected stimulus condition:
    Add condition repeated n times

Randomize schedule order

For each trial in schedule
    Run fixation
        Check button-press
    Run stimulus
        Send trigger
    If response is False, add trial back to end of schedule
```

For the continuous protocol, the trial schedule did not contain separate stimulus conditions. Instead, each trial followed the same sequence of parameter changes, the only randomization here was the duration of each stimulus. The grating started as a static low-contrast stimulus, after which the contrast was increased linearly across frames until full contrast was reached. The phase increment was then increased linearly to produce gradually increasing inward motion. Once the maximum temporal frequency had been reached, the phase increment was kept constant for the remaining frames of the stimulus presentation. See Listing 3.3 for an overview of this pipeline.

Listing 3.3: Continuous Protocol Pipeline.

```
For each frame
    If frame is within contrast ramp
        Increase contrast linearly
    Else if frame is within velocity ramp
        Increase phase step
    Else
        Keep maximum phase step
    Update phase
    Generate grating
    Draw and flip
```

Participant responses were monitored during the fixation period, as seen in Listing 3.4. A response was accepted only if it occurred within the predefined response window. Responses occurring outside of this window were classified as false and a feedback message was displayed to the participant. The missed stimulus condition was then automatically added back to the end of the schedule for the current block. The response outcome was used both to provide feedback to the participant and to determine whether the trial should be used or not in the analysis.

Listing 3.4: Button response classification.

```
Start response timer at fixation onset
Wait for button press
If press time < lower limit
    Display: Too Fast!
    log: focus = False
Else if press time within accepted interval
    Continue with next stimulation
    log: focus = True
Else if press time > upper limit
    Display: Too Slow!
    log: focus = False
```

At the beginning of each stimulus condition, the stimulation software generated an event id. Each stimulus condition corresponded to a number between one and seven. These trigger events were sent to the acquisition software and were also written into the experiment log together with the participant focus status. The experiment log also contained the chosen stimulus parameters, timing information and response outcomes. The communication method used for trigger transfer is described in the following section.

3.2.3 Synchronization & Trigger Registration

To enable integration with the MEG acquisition system, the software was designed to support synchronization through event markers corresponding to the stimulus events. This was implemented by sending a trigger at every new state from the stimulation software to the acquisition program. Since the MEG system sampled data at 1000 Hz, the trigger timing had to be accurate on a millisecond scale to ensure that stimulus onset could be aligned with the correct sample in the recorded signal.

Communication between the stimulation software and the acquisition software was implemented using the ZeroMQ library due to the importance of fast information exchange. The PUB-SUB pattern was used, where the stimulation software acted as the publisher and the acquisition software as the subscriber. This allowed the stimulation software to send trigger messages whenever the protocol changed state, without waiting for a reply from the acquisition software. This pattern was chosen instead of a request-reply structure to minimize the risk of delaying stimulus presentation. Since triggers were only sent at state transitions, the number of messages was low, reducing the risk of message loss.

Trigger messages were sent over TCP. This transport method was selected due to its reliable transportation of data, while still being sufficiently fast for the intended synchronization. TCP ensures that trigger messages arrive intact and in order, which motivated its use over the faster but less reliable UDP protocol. IPC was also considered, but this method limits the communication to one computer. In contrast, TCP allows communication between one or multiple machines. This provides flexibility

for future hardware setups. For example a setup where stimulation and acquisition are run on separate devices. The current TCP implementation is already configured to accommodate for this change.

Each stimulus condition was assigned a numerical trigger code. Fixation and baseline periods were assigned a trigger value of 0, while the stimulus conditions were assigned values between one and seven. These trigger codes allowed the recorded data to be divided into epochs corresponding to fixation, discrete stimulus conditions, and continuous stimulation periods.

Another step taken, to ensure precise alignment between the triggers and recorded MEG data, was to evaluate and account for the timing between the software trigger and the projected visual stimulus. How the delay was measured is explained in detail in section 3.4. The measured delay was used to estimate the temporal offset between the trigger and the visual stimulus. This made it possible to correct the trigger timing during analysis by shifting the trigger event according to the average measured delay.

3.3 Hardware Setup

The experimental setup consisted of the MEG measurement system, a projection-based display system, an optical mirror path and the participant setup. Since the experiment was performed in a magnetically shielded room, the hardware configuration had to allow visual stimulation while minimizing magnetic materials and electrical noise close to the MEG sensors. The visual stimulation computer and projector were therefore placed outside the magnetically shielded room, while the projected image was guided into the room using a mirror-based optical path.

3.3.1 Display System

Visual stimuli were presented using a projection-based display system. The stimulation software ran on a computer located outside the MSR, the generated image was then displayed using a BARCO FL40-WU MKII projector also positioned outside of the shielded environment. This allowed the visual stimulus to be presented to the participant without placing the projector or stimulation computer close to the sensitive MEG sensors.

The projector image was directed into the magnetically shielded room through an optical pathway consisting of two mirrors and was then displayed on a back-projection screen positioned in front of the participant. This setup was established to reduce the risk of magnetic and electrical interference while still allowing controlled presentation of high-contrast visual stimuli during MEG recordings.

Display parameters such as resolution, refresh rate, projection size and viewing distance were taken into account when defining the spatial properties of the stimulus. The stimulus size was calibrated so that the annular grating had the largest possible visual angle at the participant's viewing distance.

3.3.2 Mirror Setup

A mirror system was used to guide the projected image from the projector into the participants field of view inside the MSR. The optical path consisted of two mirrors, which directed the image from the projector, through an opening in the MSR wall and then onto the projection screen. This allowed the projector to remain outside the shielded room while the participant viewed the stimulus inside the recording environment.

The mirrors were adjusted so that the stimulus appeared centrally on the projection screen and within the participant's field of view. Alignment was executed to minimize image displacement and distortion. The image displayed on the projection screen was inverted, so the response feedback to the participants had to be adjusted in the software to compensate for this inversion. The final projected image was checked visually before recordings to ensure that the annular gratings and fixation cross were clearly visible and correctly positioned.

The projection screen was approximately 130 centimeters from the participant's eyes. This viewing distance was used when defining the spatial properties of the stimulus, including the intended visual angle of the annular gratings. The total path length from the projector to the screen was approximately 2.5 meters. These parameters, together with the constraints from the size of the MSR, yielded a visual angle of 21° for the participant. This was the largest visual angle possible in this particular environment.

3.3.3 Participant Setup

During pilot runs, the test person was seated in a comfortable chair inside the MSR with the projection screen positioned directly in front of them, see Figure 3.4 for an example. The sensor window of the MEG system was placed on the posterior part of the head approximately where the primary visual cortex is located. Participants were instructed to maintain their gaze on the center of the screen and to try and keep their focus there for the entire recording.

Behavioral responses were collected using a response button, which was a simple wired computer mouse. The mouse could be placed in the participants lap or on either armrest of the chair, it was up to the participant to choose the most comfortable placement. The participants were instructed to press the button when a fixation cross was displayed. Prior to recordings, the mouse was opened and stripped from unnecessary metal parts and functions, except for the press of the middle cursor. This was implemented to minimize electrical interference within the recording environment.

(a) (b)

Figure 3.4: Participant setup and sensor placement in the MSR. (a) Participant setup viewed from behind. The participant is looking forward toward the back-projections screen with the attention button placed in their lap. (b) Side view of the sensor placement. The sensors were placed on the occipital lobe of the head.

3.3.4 Timing Validation Setup

A photosensitive sensor was used to evaluate the timing accuracy of the projected stimulus. A small square marker was included in the projected image outside the stimulus region. The marker changed luminance together with the stimulus state, appearing white during stimulation periods and black during fixation. The sensor was positioned so that it detected the luminance changes of this marker, see Figure 3.5.

The output from the photosensitive sensor was recorded using a data acquisition (DAQ) system. This provided an independent measurement of the physical onset of the projected stimulus, which then was compared with the software trigger signal. The setup therefore allowed delays introduced by the projector and display path to be estimated.

Since the sensor and its wiring introduced an additional electrical component into the recording environment, it was only used during timing validation measurements. During MEG recordings, the photosensitive sensor was removed to reduce the risk of additional electrical noise near the MEG system.

(a) (b)

Figure 3.5: Setup used for photoresistor-based timing validation. (a) Overview of the photoresistor setup. The resistor was placed in front of where the pixel marker was located. (b) Photoresitor viewed from above. The resistor was secured in place using a velcro strap.

3.3.5 MEG System & Data Acquisition

Recordings were performed using a seven-channel high-temperature SQUID MEG system. As already mentioned, the MEG sensors were placed over the occipital region of the brain. The data was acquired using a NI-USB 6251 DAQ, as well as an amplifier. The raw brain signals could be visualized with the two oscilloscopes in the lab. The MEG data was then recorded and sent to the acquisition software on the computer. Figure 3.6 demonstrates this acquisition setup.

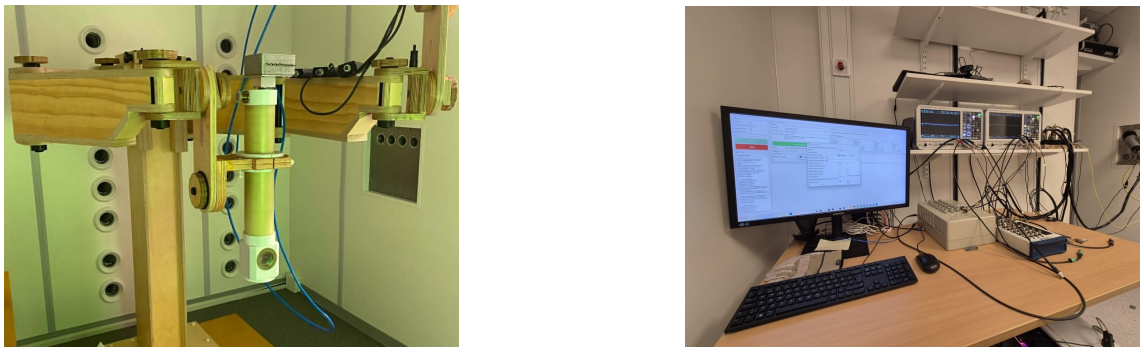

(a) (b)

Figure 3.6: MEG-acquisition hardware setup. (a) The MEG system and framework to hold it in place in the MSR. (b) Signal acquisition hardware placed outside of the MSR. This included a computer, amplifier, a DAQ and two oscilloscopes.

3.4 Pilot Testing & Validation

This section describes the assessment and validation of the developed stimulation protocols. The validation focused on three key aspects; correct presentation and visibility of the stimuli, precise timing of trigger synchronization between the stimulation and acquisition programs, and finally MEG recordings of neural activity.

3.4.1 Stimulus Presentation & Visibility

Once the stimulus hardware was in place, the visual presentation was evaluated from the intended participant position inside the MSR. The purpose of this step was to ensure that the stimulus was clearly visible, centered on the projection screen and presented without obvious distortions. To achieve this, the projector zoom, focus and image shift were adjusted together with the mirror alignment.

The geometry of the MSR limited how freely the display setup could be arranged. The projector, mirror and projection screen all had to be positioned within the available space, which restricted the optical path and image size. Because of this, the projector and mirrors were adjusted iteratively until the stimulus appeared to be centered in the participant's field of view.

Stimulus visibility was then evaluated by displaying the full protocols, including fixation cross, annular gratings, feedback messages and break images. The visuals were checked to confirm that they were clearly visible and not cut off by the projection pathway. The moving stimuli were inspected to confirm that the motion appeared smooth. This part was evaluated for different refresh rates of the projector.

In addition to the visual presentation itself, the frequency and duration of the breaks were also evaluated. The break duration was initially set to three seconds and was then gradually increased until it felt long enough to provide sufficient rest without unnecessarily interrupting the flow of the protocol. The frequency of the breaks was first tested after every fifth stimulus and was then adjusted iteratively. The aim was to identify the longest interval between breaks that still felt comfortable and manageable for the participant.

The duration of the continuous protocol was also evaluated based on perceived comfort. Since the continuous protocol contains several stimulus states within the same stimulation period, the initial assumption was that each stimulus presentation would need to be longer than in the discrete protocol. The first tested duration range was 1-3 seconds, the duration range of the discrete protocol. This interval was then gradually increased until the stimulus became uncomfortable to watch. Based on this, the maximum stimulus duration was set below the point where discomfort occurred. The lower limit was chosen to be slightly below twice the maximum stimulus duration used in the discrete protocol. This was done to allow enough time for the stimulus to change continuously while still keeping each presentation relatively short.

To evaluate the protocols more objectively in terms of stimulus presentation performance, the number of dropped frames was monitored in the software using Psy-

choPy's frameIntervals. This was incorporated into a custom function that tracked the total number of frames and the duration of each frame interval. From these values, the mean, standard deviation, minimum and maximum frame times were calculated. The frame time represents the time required for the computer to complete the calculations and scheduling needed before the next projector refresh. If this time exceeded the expected frame duration, given by 1 divided by the refresh rate, the frame was counted as a slow frame. The function therefore also tracked the total number of slow frames.

The protocols and projector refresh rates were then compared based on the ratio of slow frames to the total number of frames. This made it possible to assess which refresh rate provided the most stable stimulus presentation. The refresh rate with the best performance was then selected for the remaining timing and trigger validation.

3.4.2 Timing and Trigger Validation

Validation of trigger accuracy was investigated for both the discrete and continuous protocols, with a projector refresh rate of 60 Hz. Where software latency, end-to-end latency and trigger reliability were recorded. This was performed using several shorter sessions, each around 10 minutes long, as well as one longer session of approximately one hour to investigate long-term stability.

At the onset of every new state, a trigger message denoting the state was sent from the stimulation software to the acquisition program. These messages not only carried the trigger value, but also the time it was sent. This information was delivered to the acquisition program, which also noted the time it received the triggers. With these two time stamps the software latency was calculated for each trigger delivered during a recording. At the end of the recording, the number of triggers received, as well as mean, minimum and maximum latency were displayed in the acquisition program's log.

To evaluate the timing between the software trigger and the projected visual stimulus, a photoresistor was used. A small white square was displayed during stimulation periods and changed to black during fixation periods. The photoresistor was positioned so that it detected the luminance change of this square. By recording both the trigger signal and the photoresistor signal, the delay between the software trigger and the physical appearance of the stimulus on the screen could be estimated. This delay included the time between the software command, the display buffer update, and the actual projection of the new frame. Since the photoresistor only detected changes in screen luminance, end-to-end latency was exclusively evaluated on stimulation triggers. The photoresistor setup was only used during timing validation and was removed during MEG pilot measurements to avoid introducing additional electrical components into the magnetically shielded room.

Furthermore, trigger reliability was validated by comparing the number of triggers sent by the stimulation software with the number of triggers received by the acquisition program. This was performed to ensure the publisher-subscriber communication pattern did not result in a significant trigger loss during transmission.

Any discrepancies were interpreted as dropped messages.

3.4.3 Recording MEG Data

Before each recording session, the high-Tc SQUID sensors were cooled down and calibrated by experienced people from the research group. The quality of the cooldown and calibration was then evaluated before any experimental recordings were started. A power spectral density (PSD) noise plot was monitored in the lab to obtain an initial indication of the sensor noise level and to assess whether neural oscillatory activity was likely to be detectable. In the case of a difficult calibration, only one or a few of the SQUIDs were used for recording.

The ability to detect alpha and gamma activity was highly dependent on the noise level of the SQUID sensors. To separate neural activity from background noise, the sensor noise level had to remain below approximately 1 pT [19]. If the noise level was considered reasonable, an alpha measurement was performed as a first validation recording.

The alpha measurement consisted of a simple eyes-open/eyes-closed paradigm, where the participant alternated between keeping their eyes open and keeping their eyes closed for extended time intervals. This paradigm was used because alpha activity is expected to increase during eyes-closed periods. The recording therefore served as a practical test of whether neural activity could be observed above the sensor noise floor. The presence of a detectable alpha peak was considered a positive indication that the setup could also be used to investigate activity in other frequency bands.

Following the alpha measurement, the gamma stimulation protocol was started. Since the system was still in an early stage of development, the first gamma recordings were limited to a single stimulus condition. This reduced the complexity of the experiment and allowed the initial analysis to focus on whether gamma activity could be detected in response to visual stimulation. The recordings therefore consisted of repeated presentations of the same stimulus condition, producing a large number of epochs for later spectral and time-frequency analysis.

3.5 Data Analysis

To quantify the neural responses elicited by the stimulation protocols, the recorded MEG data was analyzed using the MNE-Python library. The first step in the analysis was to load the dataset and separate the MEG channels from the event channel. An amplitude spectrum density (ASD) plot was generated to see the general noise-levels of the recording.

A fast Fourier transform was then applied along the time axis for each MEG channel over the full recording, illustrated in Figure 3.7. This allowed the frequency content of the signal to be inspected and provided an initial indication of whether activity in the alpha or gamma frequency ranges were present.

The next step in the signal processing pipeline was filtering. A notch filter was first applied to suppress line noise at 50 Hz, as well as its harmonic at 100 Hz.

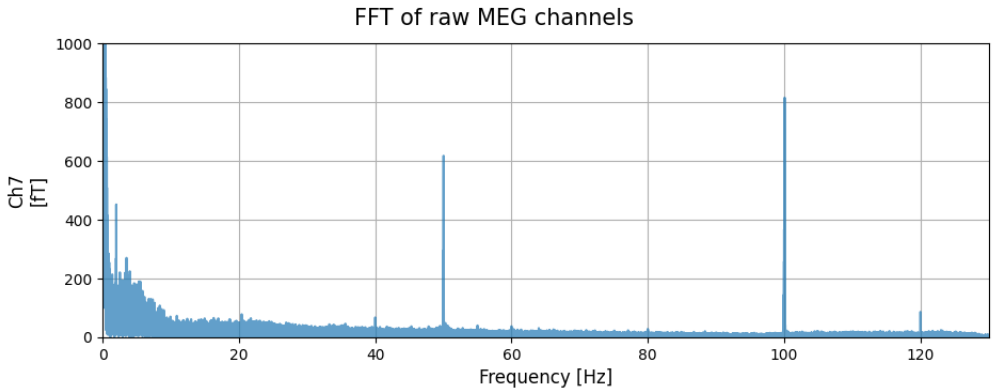

Figure 3.7: Example of a raw FFT plot from a gamma recording session.

Thereafter, a band-pass filter between 3 and 120 Hz was applied in order to retain the frequency components relevant for alpha and gamma activity. To evaluate the effect of the filtering, an FFT was also performed on the filtered data, see Figure 3.8. The dataset was then cleaned to reduce noise and other artifacts, primarily through manual annotation. During this step, excessively noisy SQUID channels were marked as bad and excluded from remaining analysis. In addition, bad data segments were annotated based on participant focus, noise or other visible artifacts.

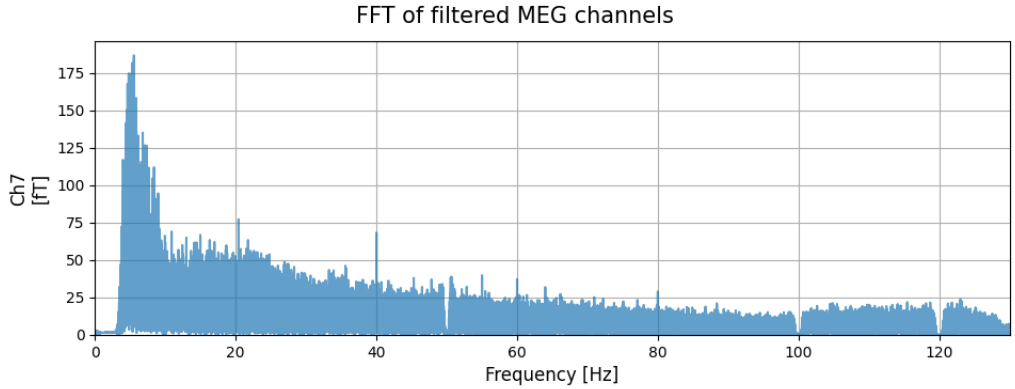

Figure 3.8: FFT of filtered data. Notch filter applied at 50, 100, 120 Hz. A bandpass filter over the range between 5-130 Hz.

Epochs were then created with a time window between -0.5 s and 1.0 s relative to stimulus onset. This was first done on the raw dataset before any cleaning and filtering was applied. This dataset was kept as a reference and is here after referred to as the uncleaned dataset. Second, epochs were created from the cleaned dataset, where noisy channels and artifact-contaminated segments had been removed. This made it possible to compare the effect of the cleaning procedure on the stimulus locked responses, also called evoked responses. The effect of the filtering and cleaning process can be observed in Figure 3.9.

For both the uncleaned and cleaned epoched datasets, evoked responses were computed for each stimulation condition. The evoked response is obtained by averaging the epochs belonging to the same stimulus condition. Butterfly plots were then

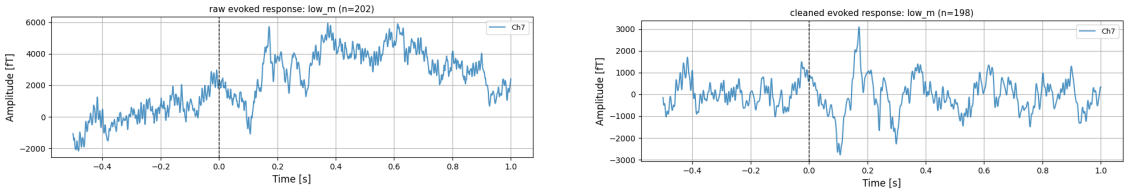

(a) (b)

Figure 3.9: Butterfly plots of the evoked responses computed from the (a) uncleaned and (b) cleaned epoched datasets. The cleaned dataset shows a more even signal, where there is a difference in amplitude between pre- and post-stimulus onset. The dashed line, at 0.0 s, denotes the start of a stimulus period.

generated for each condition in both datasets, as seen in Figure 3.9. The butterfly plots creates an overlay of the magnetic field from all of the MEG sensors, where it specifically illustrates a comparison between the pre- and post-stimulus periods. Since only one sensor was viable, there is only one signal visualized in these plots.

To focus on non-phase locked (induced) activity, the evoked response was subtracted from the individual epochs in the cleaned dataset using the MNE function subtract_evoked(). Butterfly plots were generated before and after removal of the evoked response to confirm that the phase-locked components had been removed. After subtraction, the butterfly plots were expected to be relatively flat around zero, indicating that the averaged evoked response no longer dominated the signal.

Finally, time-frequency analysis was performed on the induced activity using Morlet wavelet decomposition. This allowed stimulus-related changes in oscillatory power to be examined over both time and frequency. The analyzed frequency range was selected to include the frequencies relevant for alpha and gamma activity, i.e. 3-120 Hz. Morlet wavelets were defined using a frequency-dependent number of cycles, set to freqs/4. The number of cycles determines the trade-off between temporal and frequency resolution, where fewer cycles provide better temporal resolution but poorer frequency resolution, whereas more cycles provide better frequency resolution but poorer temporal resolution. In MNE-Python, wavelet length is determined by both the analyzed frequencies and the number of cycles, and the convolution introduces temporal smoothing related to the wavelet duration.

The value freqs/4 was chosen after testing different values in order to obtain a suitable balance between temporal resolution, frequency resolution, and robustness of the resulting time-frequency plots. Since gamma activity occurs at higher frequencies and may appear as short-lasting changes in oscillatory power, sufficient temporal resolution was prioritized. Since alpha activity occurs at lower frequencies and often changes over a longer time scale, making the same parameter choice suitable for capturing broader alpha-band changes. Power was computed for each stimulus condition and averaged across epochs. Baseline correction was applied using the pre-stimulus interval from -0.5 s to -0.1 s with a log-ratio correction, so that post-stimulus power changes were expressed relative to baseline activity.

The resulting time-frequency power was plotted separately for each channel and stimulation condition. These plots were used to assess stimulus-related channels in

alpha and gamma power over time, and to compare the responses induced by the different stimulation protocols and between recording sessions.

4

Results

In this chapter results and observations are presented for the visual stimulation software. First, the software interface is presented, followed by the two protocols. The following protocol sections contain stimulus presentation, trigger performance and MEG measurements.

4.1 Software Interface

An interface capable of adjusting the parameters of the stimulus protocols was created and used throughout the validation and subsequent MEG recordings. The window that first opens up when running the software is the main menu, see Figure 4.1. In this window, there are three protocols to choose from: continuous, discrete and localization. When hovering the mouse over each of the buttons, a short description pops up.

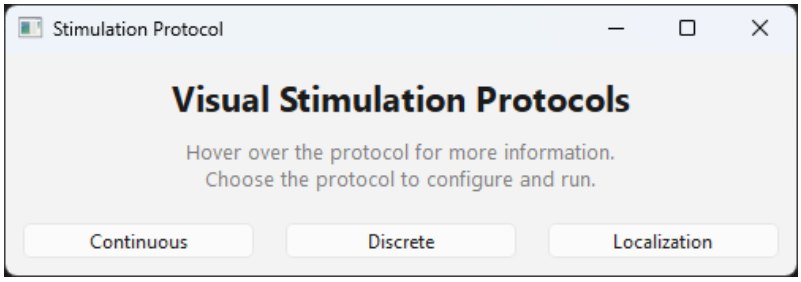

Figure 4.1: Main menu of the visual stimulation software interface. The user can choose between the continuous, discrete, and localization protocols before adjusting protocol-specific parameters.

After selecting one of the protocols, a protocol-specific parameter window opens, the windows for the discrete and continuous protocols can be seen in Figure 4.2. This window allows the user to adjust the settings used during stimulus presentation before the protocol is started. The available parameters depend on the selected protocol, but include settings such as stimulus duration, break duration, spatial frequency, temporal frequency, contrast, and the number of repetitions. This makes it possible to adapt the stimulation protocol for different validation tests and MEG recording sessions without changing the underlying code.

A localization protocol was implemented as a simplified version of the discrete protocol. In contrast to the discrete protocol, where several stimulus conditions can

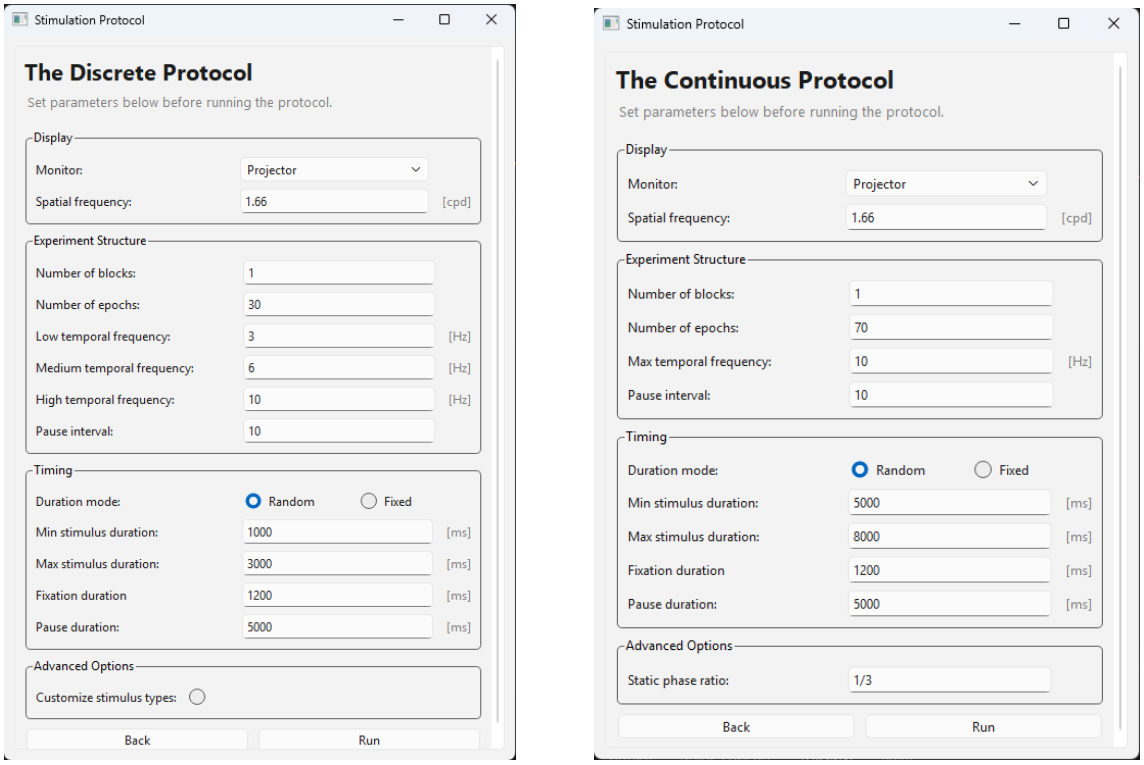

(a) (b)

Figure 4.2: Protocol-specific parameter windows in the visual stimulation software interface. (a) Parameter window for the discrete stimulation protocol, where the user can adjust settings for stimulus presentation at fixed parameter levels. (b) Parameter window for the continuous stimulation protocol, where the user can adjust settings for continuous stimulus presentation.

be presented within the same session, the localization protocol presents only one stimulus condition to the participant. The purpose of this protocol was to provide a more focused stimulation paradigm that could be used for visual cortex localization before or during MEG recordings.

The localization parameter window allows the user to adjust the main stimulus settings before starting the protocol, see Figure 4.3. These include the monitor type, spatial frequency, temporal frequency, number of epochs, stimulus duration, and fixation duration. The user can also choose whether the stimulus timing should be fixed or randomized. This makes it possible to adapt the protocol depending on the experimental needs, while keeping the stimulus presentation simple and consistent across epochs.

This protocol was designed with a larger localization procedure in mind, where the stimulus could be used to identify visually responsive sensors or regions. However, due to time constraints, only the stimulus presentation part of the localization procedure was implemented.

To then launch the visual stimulus, the user just presses the run button at the bottom of the right-hand side in the window for each of the protocols.

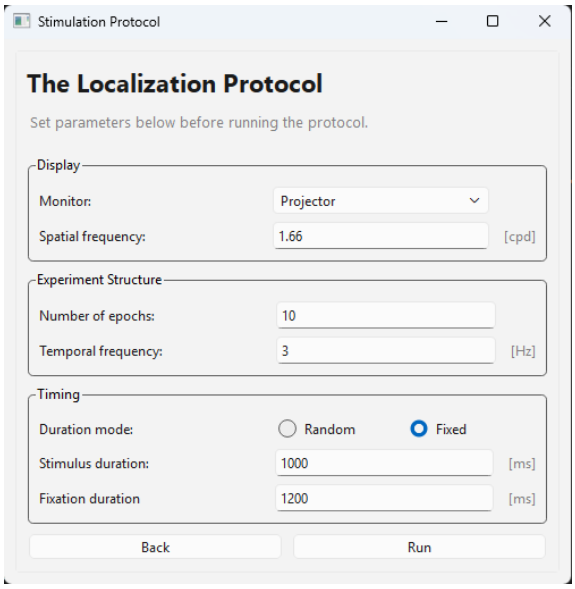

Figure 4.3: Parameter window for the localization protocol, where the stimulus settings and timing parameters can be adjusted before starting the protocol.

4.2 Discrete Protocol

The stimulus software, as described in the method, produced segments of stimulation separated by fixation crosses. An example sequence can be seen in figure 4.4. In this example four out of six stimulation types are present, as well as fixation crosses before every epoch. The two stimulation conditions not shown are the two remaining drifting gratings.

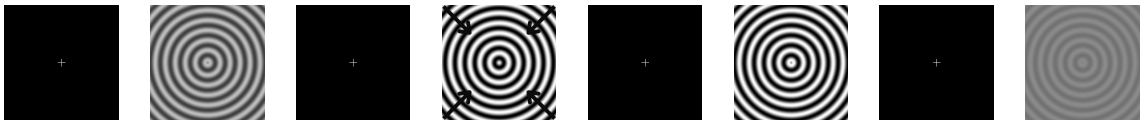

Figure 4.4: Example sequence of discrete protocol. A fixation cross begins the sequence and follows every stimulation. The stimulus as listed from left to right: medium contrast static annular grating, moving annular grating (with arrows indicating the direction of motion), high contrast static annular grating, low contrast static annular grating.

4.2.1 Stimulus Presentation & Visibility

In the assessment of frequency and duration of the break images, a duration of five seconds was considered sufficient rest from the stimulus conditions. Regarding frequency, 10 stimulation epochs was identified as the maximum tolerable interval between breaks.

The experienced stimulus presentation for the static states, including stimulus, fixation crosses and break images, did not differ between 60 and 120 Hz in refresh rate. They were displayed as expected and there was no noticeable discrepancies in

durations. The moving annular gratings performed equivalently for most epochs at the two refresh rates, where the phase increase appeared smooth and the stimulus appeared continuous. However, at 120 Hz, choppy segments were observed in a few epochs with drifting gratings.

The frame timing performance at 60, 120 and 240 Hz has been documented in Table 4.1. The mean frame duration at 60 Hz matches the expected duration, whereas for the two higher refresh rates the mean is slightly above what is expected. This is also reflected in the percentage of slow frames, as well as spikes in frame duration. In addition, the standard deviation (Std) increased with higher refresh rates, indicating more variability in frame timing at 120 and 240 Hz.

From the presented results a refresh rate of 60 Hz was chosen for the rest of the measurements for the discrete protocol.

Table 4.1: Performance of the discrete protocol at different refresh rates

Refresh rate	Mean (ms)	Std (ms)	Max (ms)	Slow frames (%)
60 Hz	16.666	0.675	36.568	0.029
120 Hz	8.542	1.445	41.579	2.42
240 Hz	4.965	1.748	27.671	15.27

4.2.2 Software Trigger Latency

The delay between sending triggers in the stimulation software to receiving them in the acquisition program was measured. No difference was observed between the shorter sessions and the long session, and these measurements have therefore been combined in Table 4.6. The requirement for the software latency was, as described in section 3.2, below 1 ms. The maximum latency is below this requirement.

Table 4.2: Measured software latency over 4626 trigger events.

Metric	Latency (ms)
Requirement	< 1.0
Mean latency	0.152
Maximum latency	0.664

4.2.3 End-to-End System Latency

The delay between when the trigger is registered and when the stimulation is projected was measured with a photoresistor. The trigger was always registered before the stimulation was actually displayed. After measured end-to-end latency, the trigger registration in the MEG acquisition software was shifted with the mean rounded to milliseconds (43 ms) to be consistent with the sampling rate.

In Table 4.3, the mean, standard deviation, as well as the 5th and 95th Percentile (Perc.) are presented. The mean latency varied some across the different sessions and the standard deviation remained relatively low. This indicates low variability in end-to-end timing for one session. However, the standard deviation for all sessions is higher. This can also be seen in the percentile range, where 90% of the delays were within a window of approximately 7 ms (39-46 ms), compared to a percentile window of around 4 ms for the individual sessions.

Table 4.3: Measured end-to-end latency over five sessions of 180 trigger events each.

Session	Mean (ms)	Std (ms)	5th Perc. (ms)	95th Perc. (ms)
Session 1	43.233	1.188	42.000	45.000
Session 2	44.206	1.232	42.000	46.000
Session 3	44.528	1.293	42.950	47.000
Session 4	40.806	1.174	39.000	43.000
Session 5	40.056	1.577	38.000	42.000
Overall	42.566	2.229	39.000	46.000

The latency can also be visualized in a plot, see Figure 4.5. A slight upward slope can be observed, along with one outlier from session 5. Sessions 1 through 3 are above sessions 5 and 6, which is corroborated with the mean latencies for the sessions in Table 4.3.

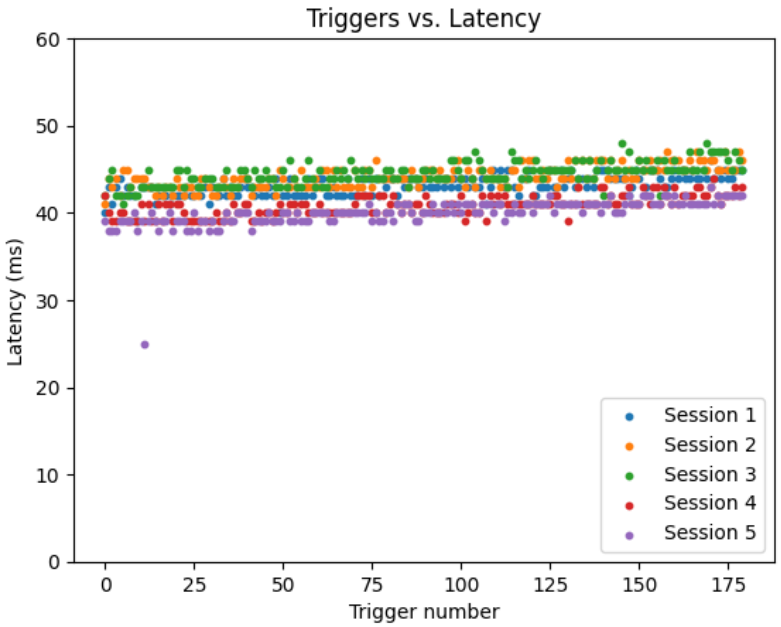

Figure 4.5: Plot depicting the five sessions mentioned in table 4.3 over the 180 trigger events.

Figure 4.6 shows a linear increase in latency over time. Here, the slope that was

somewhat visible in figure 4.5, becomes more apparent. Over time the number of outliers increases, with the data points lying below the trend. This indicates reduced long-term stability. The mean for this longer session was 50.809 ms, with a standard deviation of 5.423 ms and a 5th and 95th percentile of 43.000 ms and 60.000 ms respectively.

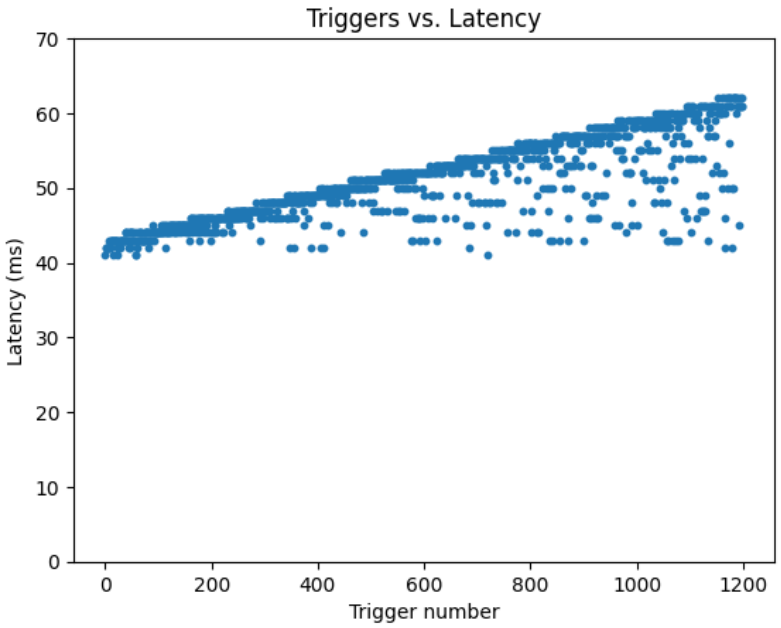

Figure 4.6: End-to-end latency over time during the hour-long session.

4.2.4 Trigger Reliability

The reliability of the publisher-subscriber pattern used for communication was assessed via the percentage of lost triggers. Table 4.4 summarizes these measurements for both the shorter recordings and the hour-long session. Since no differences were observed, the results were combined.

Table 4.4: Reliability of transmission between the stimulation software and acquisition program.

Triggers sent	4626
Triggers received	4626
Lost triggers	0%

4.2.5 Pilot MEG Measurements

From the MEG recordings that were performed, there was high variability in the resulting analyses between the different recording sessions. This section first presents the findings from the initial recording session, including both the alpha and gamma

measurements, and then moves on to the second recording session, where both alpha and gamma activity were investigated under improved recording conditions.

4.2.5.1 Recording Session with High Noise Levels

The initial recording session was conducted despite relatively high noise levels. The impact of these noise levels could be observed at multiple stages of the analysis pipeline. Firstly, the initial alpha recording displayed a clear alpha peak on the spectrum analyzer at around 11 Hz, as shown in Figure 4.7(a), indicated by the white ring. However, the ASD plot of the same data did not show the same clear peak, as shown in Figure 4.7(b), where the green highlighted area indicates the alpha frequency band. This suggests that noise may have been introduced by the recording equipment before the signal was registered on the computer.

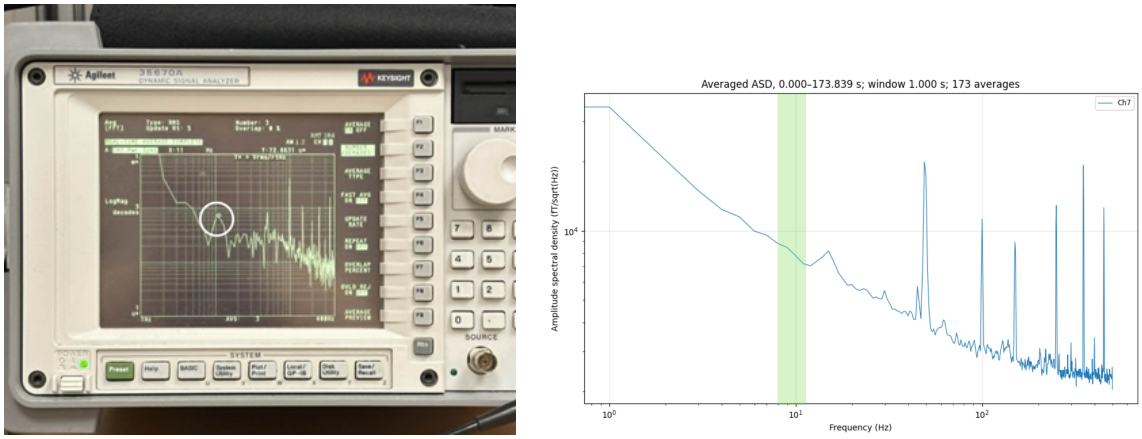

(a) (b)

Figure 4.7: Comparison between the alpha activity observed during the initial recording session and the signal registered on the computer. (a) Spectrum analyzer display, where alpha activity could be observed at around 11 Hz during the recording. The alpha peak is indicated by the white ring. (b) ASD plot of the same alpha recording, where no clear alpha peak could be identified after the signal was registered on the computer. The green area highlights where this peak should have been visible.

Since the alpha signal could be detected on the spectrum analyzer, the first gamma recording was still performed. However, the later analysis of both the alpha and gamma measurements showed no clear signs of neural activity. This can be seen in Figure 4.8, which shows the alpha time-frequency plot of two recording sessions. The first session in 4.8(a) indicates no pattern of activity in the alpha frequency band. In comparison to this, a successful alpha measurement can be observed in Figure 4.8(b), where the highest activity in the alpha frequency band is denoted by the lighter yellow intervals.

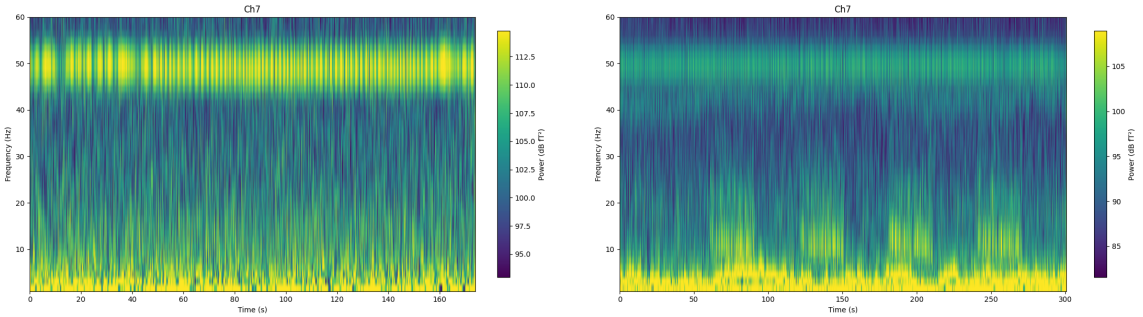

(a) (b)

Figure 4.8: Time-frequency plot of two alpha recording sessions. The power-line interference can be observed at 50 Hz. (a) Noisy recording where no neural activity can be distinguished around 8-12 Hz. (b) Successful recording where neural activity can be observed around 8-12 Hz. The lighter intervals corresponds to higher signal power obtained when the participant's eyes were closed.

For the gamma recordings, a prominent indication of excessive noise can be observed in the butterfly plot of the averaged evoked response, shown in Figure 4.9(a). In this figure, the magnitude of the signal is in the range of tens of thousands of femto-tesla. Additionally, there is no notable difference in signal behavior before and after stimulus onset. Where the stimulus onset is denoted with a dashed line at 0.0 s. This becomes even more apparent when inspecting the time-frequency plot in Figure 4.9(b), where the pre- and post-stimulus periods are divided by the dashed line at 0.0 s. Observe that there is no difference in power between the pre- and post-stimulus periods and the activity has no discernible pattern, indicating that noise is dominating. Therefore, neural activity, in any frequency band, cannot be observed.

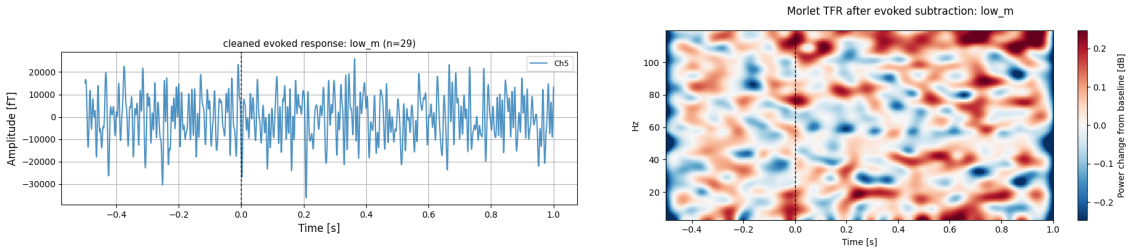

(a) (b)

Figure 4.9: Results from the initial gamma recording session with high noise levels. (a) Butterfly plot of the averaged evoked response, showing no clear difference between the pre- and post-stimulus periods, denoted by the dashed line at 0.0 s. (b) Time-frequency plot of the gamma recording, showing no clear post-stimulus gamma activity.

4.2.5.2 Gamma Recording of One Stimulus Condition

The following recording session included one stimulus condition, low_m, which was presented to the participant while data were recorded from one SQUID channel.

Two runs with different numbers of epochs were conducted, one with 500 epochs and one with 200 epochs. Overall, this session had better noise levels compared to the first recording session, as shown in Figure 4.10.

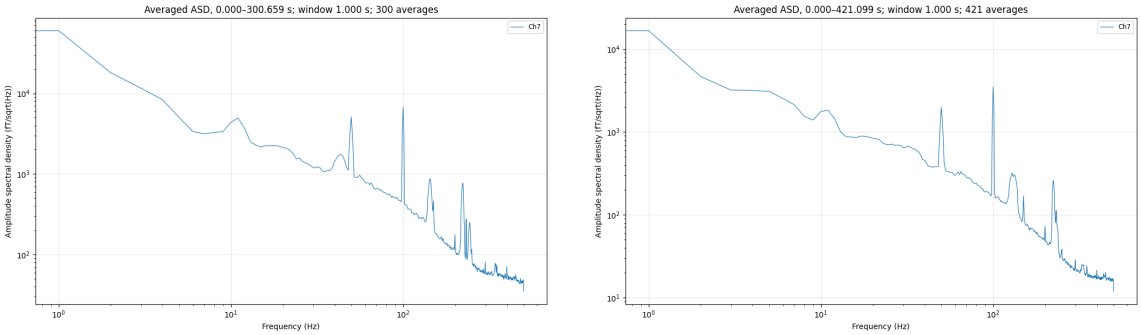

(a) (b)

Figure 4.10: ASD plots from the second recording session. (a) ASD plot from the recording with 500 epochs. (b) ASD plot from the recording with 200 epochs. Compared to the first recording session, the noise levels were lower and the recording conditions were more favorable.

The butterfly plots in Figure 4.11 show the averaged evoked responses for the 500- and 200-epoch recordings. In the 500-epoch recording, shown in Figure 4.11(a), there is a clear difference in signal amplitude when comparing the pre- and post-stimulus periods. Before stimulus onset, the signal oscillates around zero. Immediately after stimulus onset, the signal rapidly decreases in amplitude, followed by a rapid increase. After some time, the signal returns to oscillating around zero.

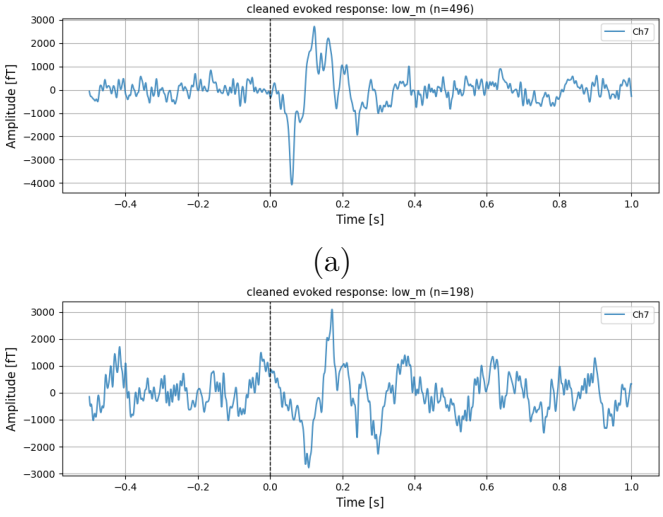

(a)

(b)

Figure 4.11: Butterfly plots of the averaged evoked responses from the second gamma recording session. The dashed line at 0.0 s denotes the stimulus onset. (a) Recording with 500 epochs, showing a clear change in amplitude after stimulus onset. (b) Recording with 200 epochs, showing a similar response pattern but with larger pre-stimulus oscillations.

The 200-epoch recording, shown in Figure 4.11(b), shows a similar overall pattern as Figure 4.11(a), where the signal rapidly decreases after stimulus onset followed by a rapid increase. However, the signal oscillations before 0.0 s and after 0.2 s shows a relatively large amplitude compared to the 500-epoch recording performed earlier the same day.

The time-frequency plots in Figure 4.12 reflect the behavior observed in the butterfly plots, where there is an evident difference in power when comparing the pre- and post-stimulus periods denoted by the dashed line at 0.0 s. In the 500-epoch recording, shown in Figure 4.12(a), there appears to be desynchronization in the beta frequency band around 15 Hz shortly after stimulus onset between 0.1 to 0.4 seconds, shown in blue. This is followed by a stronger increase in power from approximately 0.5 seconds after stimulus onset. There are also two distinct frequency bands within the gamma range that indicate increased power, located around 52 Hz and 70 Hz.

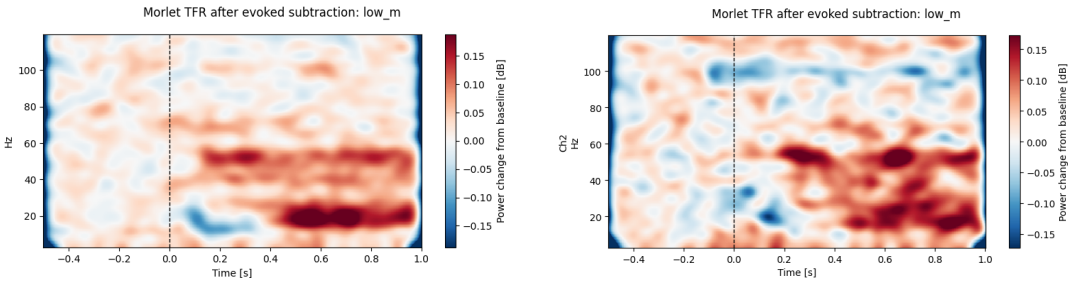

(a) (b)

Figure 4.12: Time-frequency plots from the second gamma recording session. (a) Recording with 500 epochs, showing beta-band activity around 15 Hz and increased power in the gamma range around 52 Hz and 70 Hz. (b) Recording with 200 epochs, showing less coherent activity, mainly concentrated in the beta range around 15–20 Hz and the gamma range around 55–70 Hz.

In the 200-epoch recording, shown in Figure 4.12(b), there is also a visible difference between the pre- and post-stimulus periods. However, compared to the 500-epoch recording, the pre-stimulus period appears to contain higher power, and the post-stimulus activity appears as darker, less coherent clusters across time and frequency rather than as a clearly continuous response. The main visible feature is the increase in power after stimulus onset, indicated by the red regions appearing after the dashed line at 0 s. The most prominent increase occurs in the beta frequency range, approximately 15–25 Hz, from around 0.3 s onward. A less coherent increase can also be seen in the gamma range, approximately 55–70 Hz, mainly between about 0.2 and 0.7 s after stimulus onset.

4.3 Continuous Protocol

Figure 4.13 depicts one epoch of the continuous stimulation. Note that the number of images of each state does not correspond to the duration of these. The greater part of the stimulation involves full contrast moving gratings.

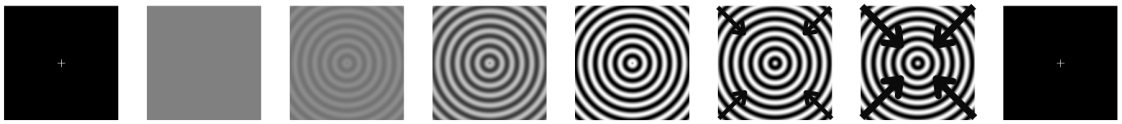

Figure 4.13: A depiction (from left to right) of one stimulation epoch in between two fixation crosses. The arrows indicate the direction of the motion and the size of them denotes the velocity.

4.3.1 Stimulus Presentation & Visibility

The same break duration and frequency were used as in the discrete protocol, with 5 seconds considered sufficient rest and 10 stimulation epochs identified as the maximum tolerable interval between breaks. In a similar fashion, the duration of the continuous stimulus was evaluated, where the minimum duration was 5 seconds and the maximum was 8 seconds.

The experienced stimulus presentation for the first part of the stimulation epoch, where the contrast is increased from no contrast to full contrast, was perceived as smooth with no hiccups at both 60 and 120 Hz. The second part, where the velocity increases linearly, appeared smooth at 60 Hz but discrepancies were observed for many of the epochs at 120 Hz. This included abrupt increases in velocity and occasional deviations from the intended constant acceleration.

Frame timing statistics at 60, 120 and 240 Hz is recorded in Table 4.5. Here, the mean frame duration matches the expected duration at 60 and 120 Hz, whereas the mean duration at 240 Hz exceeds what is expected. This deviation is also reflected in standard deviation, maximum frame duration and percentage of slow frames.

From the presented results a refresh rate of 60 Hz was chosen for the rest of the measurements for the continuous protocol.

Table 4.5: Performance of the continuous protocol at different refresh rates

Refresh rate	Mean (ms)	Std (ms)	Max (ms)	Slow frames (%)
60 Hz	16.666	0.636	33.356	0.0084
120 Hz	8.341	0.402	18.369	0.12
240 Hz	5.847	1.129	23.241	0.78

4.3.2 Software Trigger Latency

As with the discrete protocol, the continuous protocol exhibited the same patterns for software latency. Accordingly, the measurements from the different sessions were combined in Table 4.6. The latency requirement was met for this protocol as well.

Table 4.6: Measured software latency over 1876 trigger events.

Metric	Latency (ms)
Requirement	< 1.0
Mean latency	0.147
Maximum latency	0.389

4.3.3 End-to-End System Latency

End-to-end latency was measured in the same way as for the discrete protocol. The measurements for the five shorter sessions have been summarized in table 4.7. The mean latency varied between 40 and 43 ms for the different sessions. The standard deviation stayed quite consistent around 1 ms. This was also reflected in the percentile range, where 90 % of the delays were within 4 ms (40-44 ms) of each other.

Table 4.7: Measured end-to-end latency over five sessions of 70 trigger events each.

Session	Mean (ms)	Std (ms)	5th Perc. (ms)	95th Perc. (ms)
Session 1	42.857	1.004	41.450	44.000
Session 2	42.871	1.107	41.000	45.000
Session 3	40.314	0.871	39.000	41.550
Session 4	41.386	1.073	40.000	43.000
Session 5	42.943	1.157	41.000	45.000
Overall	42.074	1.487	40.000	44.000

For a visual representation of the four shorter sessions Figure 4.14 can be inspected. As with the discrete protocol, an upward slope can be identified. All data points are confined around 40 ms and no clear outliers can be observed.

Long-term stability of end-to-end latency was assessed and can be seen in Figure 4.15. The same trend as for the discrete protocol can be observed here, where the increase in latency has a linear behavior. A few data points can be seen as outliers, where most of them can be found in the second half of the plot. These outliers are found under the slope. The mean latency of the hour-long session was 44.385 ms, with a standard deviation of 2.455 ms, and a 5th and 95th percentile of 41.000 ms and 49.000 ms respectively.

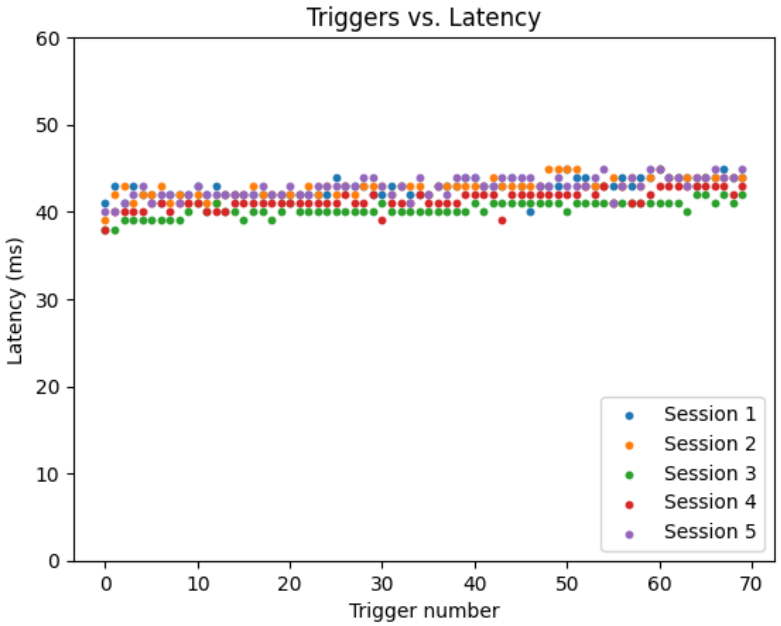

Figure 4.14: Plot depicting the five sessions mentioned in table 4.7 over the 70 trigger events.

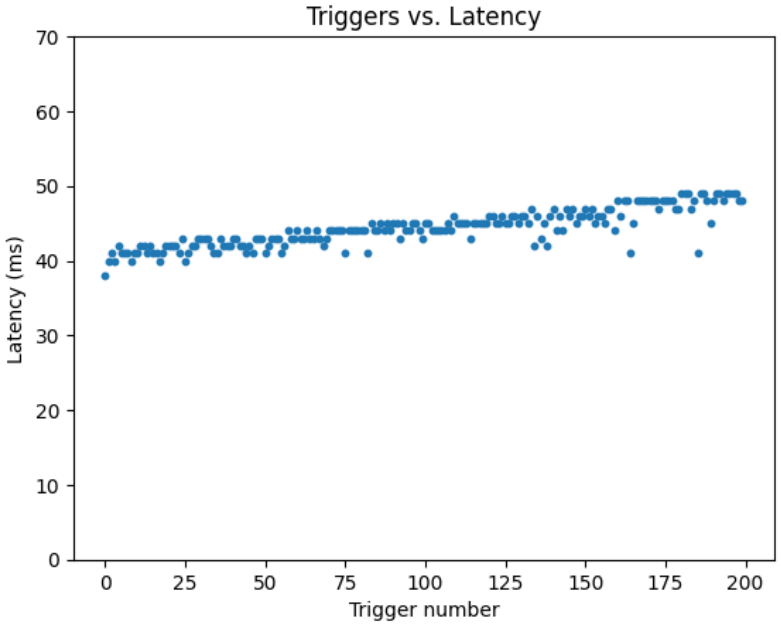

Figure 4.15: End-to-end-latency over time during the hour-long session.

4.3.4 Trigger Reliability

Trigger reliability of the continuous protocol looked identical to the discrete protocol. Accordingly, the shorter sessions and the hour-long recording were combined and documented in Table 4.8. The number of triggers sent from the stimulation software matched the number received by the acquisition program.

Table 4.8: Reliability of transmission between the stimulation software and acquisition program.

Triggers sent	1876
Triggers received	1876
Lost triggers	0%

4.4 Stimulus Display Setup

The resulting display setup in this project consisted of a projector, two mirrors and a back-projection screen. The projector positioning can be seen in Figure 4.16. It can be noted that the entire projected image does not fit through the hole. This was accounted for by adjusting the size of the stimulus window as well as the projector focus, zoom and shift.

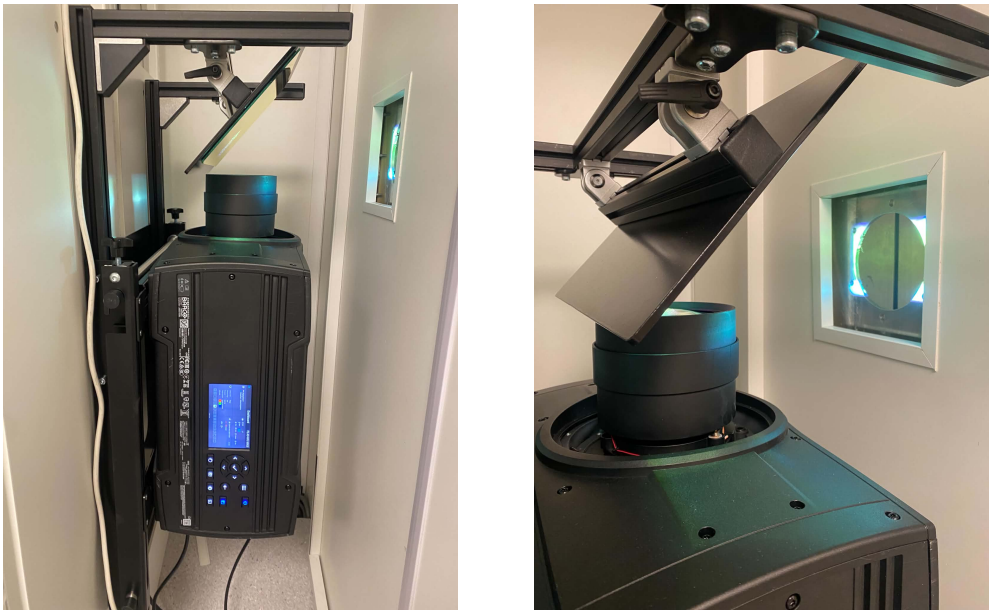

(a) (b)

Figure 4.16: The projector mounted outside of the MSR. It is pointed upward toward a mirror, which in turn guides the projected image through the hole in the wall. (a) Projector positioning. (b) Light beam projected through the hole in the MSR wall.

Figure 4.17 shows how the projected image travels into the MSR to the back-projection screen. The back-projection screen was positioned as far from the mirror as possible in order to maximize the visual angle, which reached 21° for the participant. The placement of the back-projection screen was restricted by the MEG-mount, as well as the chair the participant needed to sit in.

(a) (b)

Figure 4.17: The mirror display system, where the light beam from the projector is transported to the back-projection screen. (a) The mirror, angled at 45°, receives the light beam from the hole through the MSR wall. (b) The back-projection screen displaying an image of a forest.

5

Discussion & Conclusions

This chapter discusses the results of each of the protocols separately, then moves on to discuss the hardware setup as well as future work that can be expanded upon the findings and discussions. Lastly, conclusions are drawn.

5.1 Discrete Protocol

The discrete protocol was designed to display different stimulus conditions in a randomized order to induce gamma activity. In order for the protocol to be compatible with the MEG acquisition software, frame and trigger timing had to be accurate and reliable. This section presents further discussions regarding the evaluation of the discrete protocol, as well as the performed MEG recordings.

5.1.1 Frame Timing and Perceived Stimulus Smoothness

Both experienced stimulus presentation and frame timing was considered when deciding on which refresh rate to use for displaying the protocol. Although 120 Hz provided mostly smooth drifting gratings, 60 Hz resulted in a better percentage of dropped frames. The dropped-frame rate at 120 Hz reached 2.42 %, which was considered too high for this application. Furthermore, the standard deviation more than doubled at 120 Hz compared to 60 Hz.

5.1.2 Trigger Latency & Reliability

The software latency for transmission of triggers never exceeded 1 ms in the measurements performed. This was within the desired latency. However, when assessing end-to-end system latency, it was discovered that the display system introduces an additional delay. In shorter sessions, this can be compensated for by adding the mean delay to the time when registering triggers. As a result, 90 % of the triggers registered within 7 ms of the stimulus being displayed, which is less than a frame. This was considered acceptable for pilot testing, although the desired target is still to maintain a latency below 1 ms. Achieving this would require further development to improve accuracy.

This becomes especially apparent during the hour-long session performed with the photoresistor. This could be due to asynchrony between computer and projector as well as the internal processing of the projector. The delay could be mitigated

by accounting for the linear increase in latency over time. However, due to the increasing number of outliers, this would still result in high variability in trigger timing relative to the displayed stimuli.

From the transmission reliability validation that was performed, there appeared to be no issues with the publisher-subscriber pattern chosen for communication. This was expected due to the relatively low trigger frequency during transmission. However, further measurements may be necessary to obtain a more robust estimate of trigger reliability.

5.1.3 MEG Recordings

The MEG recordings performed with the discrete protocol provided several important observations regarding the stimulus protocol's ability to induce gamma-band activity. Overall, the results suggest that gamma activity could be observed under improved recording conditions.

In the initial recording session, the noise levels of the acquisition setup had a significant effect on the resulting signals. Clear alpha activity could be observed on the spectrum analyzer, while the same activity could not be clearly identified in the PSD plotted on the computer, see Figure 4.7. This suggests that the SQUID noise levels may have been low enough to detect neural activity, but that additional noise was introduced when the signal passed through the DAQ to the computer. Since this additional noise covered the otherwise visible alpha activity, detecting gamma activity became even more difficult. This is especially relevant because gamma activity can have a lower magnitude than alpha activity. Therefore, the first recording did not provide favorable conditions for evaluating whether the protocol could reliably induce gamma oscillations.

The second recording session provided more favorable conditions for gamma analysis, see Figure 4.10. Although the noise levels in the ASD plot were still relatively high, an amplifier with an amplification factor of 20 was used to amplify the SQUID signals before they were passed to the DAQ. This made neural activity much clearer in the analysis, which was especially evident from the prominent alpha activity in the generated time-frequency plots. Under these improved recording conditions, the gamma stimulation protocol showed some induced post-stimulus activity in the gamma frequency band, around 52 and 70 Hz. This suggests that the developed discrete stimulation protocol was capable of eliciting measurable gamma-band activity in the visual cortex.

However, the strongest observed response in the second recording session was not in the gamma band, but in the beta frequency band. The time-frequency results showed clear beta activity, while the gamma activity was present but less prominent. This differs from the typical response pattern described in visually induced gamma studies, where gamma power increases while alpha power decreases. After consultation with our supervisor, this beta-activity was determined to be unusual but not unexpected. A strong beta response may indicate that the brain is trying to block bottom-up signaling, which is a process driven by external stimuli, or it could also be beta-rebound. This strong beta-activity may therefore have made

it more difficult to clearly observe the expected gamma increase. Although some gamma-activity was still observed.

The number of epochs included in the analysis also seemed to affect how clearly the stimulus-related activity could be observed. In the second recording session, analyses were performed using both 500 and 200 epochs. The analysis based on 500 epochs elicited clearer activity than the analysis based on fewer epochs. This is expected, since a larger number of epochs can improve the signal-to-noise ratio by enhancing activity that is time-locked or consistently induced by the stimulus, while reducing random noise through averaging.

With these points in mind, the results suggest that the discrete stimulation protocol was able to elicit measurable gamma responses in the MEG recordings, see Figure 4.12. However, the clarity of the gamma activity depended strongly on the recording conditions, particularly noise level and signal amplification. Further recordings, including all stimulus conditions and different numbers of epochs, are therefore needed to evaluate the reliability of the protocol and determine how many epochs are required to consistently detect gamma-band activity.

5.2 Continuous Protocol

The continuous protocol was designed to display a single epoch type containing multiple stimulus conditions. To enable experimental use it had to be compatible with the MEG acquisition software and hardware, similarly to the discrete protocol. This section therefore discusses the overall performance in terms of frame timing and trigger latency and reliability.

5.2.1 Frame Timing and Perceived Stimulus Smoothness

The frame timing measurements performed on the continuous protocol showed good results at both 60 and 120 Hz, where the mean frame duration, standard deviation and percentage of dropped frames were within acceptable limits. However, the experienced stimulus presentation did not fully reflect these results. This is believed to be due to the use of constant acceleration rather than constant velocity for the moving gratings. As a result, dropped frames may become more noticeable because the velocity changes more abruptly over time.

5.2.2 Trigger Latency & Reliability

As with the discrete protocol, the added display-system latency was the main issue in the continuous protocol. The mean end-to-end system latency varied somewhat but 90 % of the data points remained within a 4 ms window. Adding the mean latency to the acquisition system would therefore register most of the triggers within 2 ms of the displayed stimulus.

During the hour-long session performed with the photoresistor, the latency showed a gradual increase over time. Which again could be due to asynchrony between computer and projector as well as the internal processing of the projector. While

this could be partially mitigated by accounting for a linear drift in latency, multiple hour-long sessions would have to be recorded for a robust estimate of the slope.

5.2.3 MEG Recordings

Due to the limited number of recording sessions, and the time required to detect gamma activity from the discrete protocol, MEG measurements have not yet been performed for the continuous protocol. Therefore, the ability of the continuous protocol to induce gamma-band activity could not be evaluated within the scope of this thesis. However, since the discrete protocol, together with the existing MEG acquisition system, was able to elicit detectable gamma activity, there are encouraging indications that the continuous protocol may also be capable of inducing gamma-band activity.

5.3 Comparison

Both the discrete and continuous protocol performed optimally at a refresh rate of 60 Hz, although the advantage manifested differently for the two. The continuous protocol demonstrated acceptable frame timing at 120 Hz in Table 4.5, but visual inspection suggested insufficient stability in stimulus presentation. The discrete protocol, on the other hand, showed greater issues with frame timing, although discrepancies in stimulus presentation were also observed. One explanation for this is the design of the stimulus, where constant acceleration is only present in the continuous protocol. This suggests that the continuous design may be less robust to jitter.

The software trigger latency and reliability do not differ between the two protocols and can be attributed to the stimulation software as a whole rather than protocol design. Regarding end-to-end latency, both protocols exhibit a linear increase over time between trigger registration and stimulus display. The variability appears to be less for the continuous protocol, which can be seen for the shorter sessions.

Comparing the hour-long sessions, further confirms this, where the main difference is the amount of outliers under the slope, see Figures 4.6 and 4.15. For the continuous protocol it seems possible to adjust for the increase in latency over time, whereas doing this for the discrete protocol would result in a high variability. For optimal use of the two protocols, multiple shorter sessions appear to provide better trigger accuracy, whereas a single longer session tends to reduce accuracy.

5.4 Hardware Setup

The stimulus presentation hardware was an important part of the experimental setup, since the visual stimuli had to be delivered in a way that was visible to the participant while remaining compatible with the MEG environment. The setup consisted of a projector, two mirrors and a back-projection screen. These allowed the stimulus to be presented inside the MSR without creating interference with the

MEG sensors.

The main limitation of this setup was that the projector was too large in depth to fit horizontally in its designated position outside the MSR. The projector lens was initially intended to align directly with the opening in the MSR wall, but this was not possible due to the size of the projector. Instead, the projector had to be angled upward toward a mirror, which then had to be adjusted to direct the projection through the opening in the MSR wall.

This created practical challenges during setup, especially because the projected image increases in size with distance. As a result, there were limitations on how large a visual angle the system could display. This is relevant since the literature study indicated that a larger visual angle can elicit a stronger gamma response. Although parts of the full projected screen were cut off by the opening in the MSR wall, the stimulus itself was not disrupted, as the stimulus window was adjusted to fit within the visible area passing through the opening.

Overall, the stimulus presentation hardware was functional and allowed the visual stimuli to be presented inside the MSR, but the setup was less flexible than initially intended. The need to project via a mirror introduced additional alignment requirements and limited the maximum visual angle that could be displayed.

5.5 Future

One possible solution for reducing end-to-end latency in longer recordings would be to permanently include a photodiode as part of the hardware setup. The photodiode would need to be shielded to mitigate electrical interference, but it could provide improved accuracy in trigger timing. A photodiode with luminance sensitivity, capable of differentiating between luminance levels could be used to register different stimuli. The different luminance levels would encode the stimulus conditions.

Future MEG measurements would also need to be performed using the continuous protocol to determine if it can induce any gamma activity. Since the continuous protocol gradually changes stimulus parameters over time, it is therefore important to determine whether each stimulation period is long enough for gamma-band activity to emerge and be detected in the MEG signal. This would help establish whether the current duration used in the protocol is sufficient, or whether longer stimulation periods are needed to obtain stable and measurable gamma responses.

Another aspect requiring further evaluation is the design of the continuous stimulation epochs. In the current implementation, the stimulus is defined by a linear increase in both contrast and motion velocity within each stimulation period. However, alternative ways of modulating contrast and velocity over time should be investigated and validated during future MEG recordings.

In particular, the optimal relationship between the contrast-increase and the velocity-increase remains unclear. In the present design, the first third of the minimum stimulus duration is allocated to a linear increase in contrast, while the remaining two thirds are allocated to a linear increase in motion velocity. This division was chosen to prioritize motion duration, based on previous findings indicating that

high-contrast moving gratings elicit stronger gamma-band responses. However, this fixed partition may not be optimal. Future work should therefore investigate different distributions between contrast and velocity, as well as alternative non-linear or step-wise transitions, to determine whether these modifications improve the robustness or strength of induced gamma-band activity in MEG recordings.

Future work on the localization protocol could also be of interest. Since the current MEG system has a low number of sensors, advanced source localization cannot be performed in the same way as with a whole-head sensor system. One idea that was brainstormed and explored was therefore to create a manual localization protocol. This would combine the stimulus software with a simplified real-time, or near-real-time, signal processing approach to indicate whether strong gamma activity was present at the current sensor location.

The protocol could then be run iteratively, where the sensor placement is adjusted between recordings until a suitable position is found. Some initial attempts were made to create a simple real-time signal processing method, synchronized with the stimulus events, for this purpose. However, since it was in such an early development stage, it was not fully functional and was therefore not included in the report. Only the interface for the localization protocol was included, to indicate that this could be the next step when it comes to performing MEG recordings.

5.6 Conclusions

In conclusion, a stimulation software consisting of static and moving annular gratings was successfully implemented and shown to be compatible with MEG measurements. The system allowed for acquisition and analysis of neural responses, including visually induced oscillatory activity in the alpha, beta and gamma frequency ranges.

Furthermore, two distinct stimulation protocols, referred to as discrete and continuous, were implemented within the same software framework. Both protocols were successfully executed under MEG-compatible conditions, although they exhibited different performance characteristics with respect to frame timing, stimulus stability and sensitivity to jitter.

In terms of performance during piloting, the continuous protocol showed more stable frame timing at higher refresh rates, although it was only evaluated in terms of stimulus presentation and timing performance and not in MEG recordings. As a result, direct comparison with the discrete protocol in terms of neural outcomes is not possible. Neither protocol was conclusively superior, as MEG piloting was only performed for the discrete protocol.

The hardware setup was sufficient to present visual stimuli inside the MEG environment without introducing observable interference in the measured neural signals. However, additional sources of noise were introduced during signal transfer from the SQUID system through the DAQ to the recording computer, which affected signal clarity.

Regarding temporal accuracy, both stimulus presentation and MEG acquisition were successfully synchronized. However, both protocols were affected by end-to-end la-

tency introduced by the display system. While short sessions achieved acceptable accuracy (with 90 % of triggers within 3 ms of stimulus presentation), longer sessions exhibit increasing latency drift, indicating limitations for extended recordings without additional correction mechanisms.

Finally, validation through pilot testing indicate that the discrete protocol is capable of inducing gamma-band activity in the visual cortex. The continuous protocol could not be evaluated with MEG-recordings within the scope of this thesis. However, system performance and stimulus design indicate that it may also be capable of inducing measurable oscillatory responses.

References

[1] E. R. Kandel, *Principles of Neural Science*, 5th ed. New York ; Toronto: McGraw-Hill Medical, 2013.

[2] G. Buzsáki. "Neural oscillation | definition, types & synchronization," Encyclopaedia Britannica, Accessed: Jan. 30, 2026. [Online]. Available: https://www.britannica.com/science/brain-wave-physiology.

[3] E. Garcia-Rill, *Waking and the Reticular Activating System in Health and Disease*. Academic Press, 2015.

[4] E. V. Orekhova et al., "Input-dependent modulation of meg gamma oscillations reflects gain control in the visual cortex," *Scientific Reports*, vol. 8, no. 1, May 2018. DOI: 10.1038/s41598-018-26779-6.

[5] E. V. Orekhova et al., "Neural gain control measured through cortical gamma oscillations is associated with sensory sensitivity," *Human Brain Mapping*, vol. 40, no. 5, pp. 1583–1593, 2019. DOI: https://doi.org/10.1002/hbm.24469. eprint: https://onlinelibrary.wiley.com/doi/pdf/10.1002/hbm.24469. [Online]. Available: https://onlinelibrary.wiley.com/doi/abs/10.1002/hbm.24469.

[6] E. V. Orekhova, A. O. Prokofyev, A. Y. Nikolaeva, J. F. Schneiderman, T. A. Stroganova, and C. Rennò-Costa, "Additive effect of contrast and velocity suggests the role of strong excitatory drive in suppression of visual gamma response," *PLOS ONE*, vol. 15, no. 2, Feb. 2020. DOI: 10.1371/journal.pone.0228937.

[7] E. V. Orekhova et al., "Spatial suppression in visual motion perception is driven by inhibition: Evidence from meg gamma oscillations," *NeuroImage*, vol. 213, p. 116 753, 2020, ISSN: 1053-8119. DOI: https://doi.org/10.1016/j.neuroimage.2020.116753. [Online]. Available: https://www.sciencedirect.com/science/article/pii/S1053811920302408.

[8] "Magnetoencephalography | imaging technique," Encyclopaedia Britannica, Accessed: Jan. 30, 2026. [Online]. Available: https://www.britannica.com/topic/magnetoencephalography.

[9] S. P. Singh, "Magnetoencephalography: Basic principles," *Annals of Indian Academy of Neurology*, vol. 17, no. Suppl 1, S107–S112, 2014. DOI: 10.4103/0972-2327.128676.

[10] S. Muthukumaraswamy and K. Singh, "Visual gamma oscillations: The effects of stimulus type, visual field coverage and stimulus motion on meg and eeg recordings," *NeuroImage*, vol. 69, pp. 223–230, 2013, ISSN: 1053-8119. DOI: https://doi.org/10.1016/j.neuroimage.2012.12.038. [On-

line]. Available: https://www.sciencedirect.com/science/article/pii/S1053811912012232.

[11] G. Buzsáki, *Rhythms of the Brain*. Oxford University Press, 2006.

[12] R. Wu et al., "Electroacupuncture stimulation to modulate neural oscillations in promoting neurological rehabilitation," *Brain Research*, vol. 1822, p. 148 642, 2024, ISSN: 0006-8993. DOI: https://doi.org/10.1016/j.brainres.2023.148642. [Online]. Available: https://www.sciencedirect.com/science/article/pii/S0006899323004134.

[13] F. L. da Silva, "Eeg and meg: Relevance to neuroscience," *Neuron*, vol. 80, no. 5, pp. 1112–1128, 2013, ISSN: 0896-6273. DOI: https://doi.org/10.1016/j.neuron.2013.10.017. [Online]. Available: https://www.sciencedirect.com/science/article/pii/S0896627313009203.

[14] A. R. Longo, N. Bolognini, and L. Zapparoli, "Shaping gamma oscillations through sensory stimulation: A systematic review in healthy adults," *Biological Psychology*, vol. 204, p. 109 211, 2026, ISSN: 0301-0511. DOI: https://doi.org/10.1016/j.biopsycho.2026.109211. [Online]. Available: https://www.sciencedirect.com/science/article/pii/S0301051126000244.

[15] J. Veit, G. Handy, D. P. Mossing, B. Doiron, and H. Adesnik, "Cortical vip neurons locally control the gain but globally control the coherence of gamma band rhythms," *Neuron*, vol. 111, no. 3, 405–417.e5, 2023, ISSN: 0896-6273. DOI: https://doi.org/10.1016/j.neuron.2022.10.036. [Online]. Available: https://www.sciencedirect.com/science/article/pii/S0896627322009965.

[16] J. B. Swettenham, S. D. Muthukumaraswamy, and K. D. Singh, "Spectral properties of induced and evoked gamma oscillations in human early visual cortex to moving and stationary stimuli," *Journal of Neurophysiology*, vol. 102, no. 2, pp. 1241–1253, 2009, PMID: 19515947. DOI: 10.1152/jn.91044.2008. eprint: https://doi.org/10.1152/jn.91044.2008. [Online]. Available: https://doi.org/10.1152/jn.91044.2008.

[17] O. David, J. M. Kilner, and K. J. Friston, "Mechanisms of evoked and induced responses in meg/eeg," *NeuroImage*, vol. 31, no. 4, pp. 1580–1591, 2006, ISSN: 1053-8119. DOI: https://doi.org/10.1016/j.neuroimage.2006.02.034. [Online]. Available: https://www.sciencedirect.com/science/article/pii/S1053811906001170.

[18] G. Arcara, G. Pellegrino, A. Pascarella, D. Mantini, E. Kobayashi, and K. Jerbi, *Psychophysiology Methods*. New York, NY: Springer US, 2024, ISBN: 978-1-0716-3545-2. DOI: 10.1007/978-1-0716-3545-2_8. [Online]. Available: https://doi.org/10.1007/978-1-0716-3545-2_8.

[19] J. F. Schneiderman, S. Ruffieux, C. Pfeiffer, and B. Riaz, "On-scalp meg," in *Magnetoencephalography*, S. Supek and C. Aine, Eds., Cham: Springer, 2019. DOI: 10.1007/978-3-030-00087-5_78. [Online]. Available: https://doi.org/10.1007/978-3-030-00087-5_78.

[20] MNE-Python Developers, *Overview of meg/eeg analysis with mne-python*, https://mne.tools/stable/auto_tutorials/intro/10_overview.html, MNE-Python 1.12.1 documentation. Accessed: 2026-05-12, 2025.

[21] MNE-Python Developers, *Preprocessing*, https://mne.tools/stable/auto_tutorials/preprocessing/index.html, MNE-Python documentation, accessed 16 May 2026.

[22] MNE-Python Developers, *Segmenting continuous data into epochs*, https://mne.tools/stable/auto_tutorials/epochs/index.html, MNE-Python documentation, accessed 16 May 2026.

[23] MNE-Python Developers, *Estimating evoked responses*, https://mne.tools/stable/auto_tutorials/evoked/index.html, MNE-Python documentation, accessed 16 May 2026.

[24] MNE-Python Developers, *Time-frequency analysis*, https://mne.tools/stable/auto_tutorials/time-freq/index.html, MNE-Python documentation, accessed 16 May 2026.

[25] R. H. Wurtz, *Brain circuits for visually guided saccades*, [Image]. Wikimedia Commons, Licensed under CC BY 4.0. Accessed: May 16, 2026, 2015. [Online]. Available: https://commons.wikimedia.org/w/index.php?curid=44179843.

[26] S. Muthukumaraswamy and K. Singh, "Visual gamma oscillations: The effects of stimulus type, visual field coverage and stimulus motion on meg and eeg recordings," *NeuroImage*, vol. 69, pp. 223–230, 2013, ISSN: 1053-8119. DOI: https://doi.org/10.1016/j.neuroimage.2012.12.038. [Online]. Available: https://www.sciencedirect.com/science/article/pii/S1053811912012232.

[27] R. L. DeValois and K. K. DeValois, *Spatial Vision*. Oxford University Press, 2000.

[28] J. W. Peirce et al., "Psychopy2: Experiments in behavior made easy," *Behavior Research Methods*, vol. 51, pp. 195–203, 2019. DOI: 10.3758/s13428-018-01193-y.

[29] IBM, *The interprocess communication (ipc) overview*, Modified date: 17 June 2018. Accessed: 2026-05-11, Jun. 2018. [Online]. Available: https://www.ibm.com/support/pages/interprocess-communication-ipc-overview.

[30] ZeroMQ Project, *Zmq_ipc — zeromq ipc transport*, Accessed: 2026-05-26, 2017. [Online]. Available: http://api.zeromq.org/4-2:zmq-ipc.

[31] IBM, *Transmission control protocol/internet protocol*, IBM AIX 7.3 Documentation, Accessed: 2026-05-26, 2024. [Online]. Available: https://www.ibm.com/docs/en/aix/7.3.0?topic=management-transmission-control-protocolinternet-protocol.

[32] Khan Academy, *The problems with packets*, Accessed: 2026-05-11, n.d. [Online]. Available: https://www.khanacademy.org/computing/computers-and-internet/xcae6f4a7ff015e7d:the-internet/xcae6f4a7ff015e7d:transporting-packets/a/the-problems-with-packets.

[33] Khan Academy, *User datagram protocol (udp)*, Accessed: 2026-05-11, n.d. [Online]. Available: https://www.khanacademy.org/computing/computers-and-internet/xcae6f4a7ff015e7d:the-internet/xcae6f4a7ff015e7d:transporting-packets/a/user-datagram-protocol-udp.

[34] J. Postel, *Transmission Control Protocol*, RFC 793, Accessed: 2026-05-11, Sep. 1981. [Online]. Available: https://www.rfc-editor.org/rfc/rfc793.html.

[35] ZeroMQ. "Ømq: The guide." Accessed: May. 4, 2026. [Online]. Available: https://zguide.zeromq.org.

[36] R. C. Limited, *Pyqt6*, 2025. [Online]. Available: https://pypi.org/project/PyQt6/.

DEPARTMENT OF ELECTRICAL ENGINEERING
CHALMERS UNIVERSITY OF TECHNOLOGY
Gothenburg, Sweden
www.chalmers.se

CHALMERS
UNIVERSITY OF TECHNOLOGY